HHS Public Access

Author manuscript

Nature. Author manuscript; available in PMC 2020 April 09.

Published in final edited form as:

Nature. 2019 October ; 574(7778): 413–417. doi:10.1038/s41586-019-1641-1.

Population imaging of neural activity in awake behaving mice

Kiryl D. Piatkevich[1,2,*], **Seth Bensussen**[3,*], **Hua-an Tseng**[3,*], **Sanaya N. Shroff**[3], **Violeta Gisselle Lopez-Huerta**[4], **Demian Park**[1,2], **Erica E. Jung**[1,5], **Or A. Shemesh**[1,2], **Christoph Straub**[6], **Howard J. Gritton**[3], **Michael F. Romano**[3], **Emma Costa**[1], **Bernardo L. Sabatini**[6], **Zhanyan Fu**[4], **Edward S. Boyden**[1,2,7,8,9,10,†], **Xue Han**[3,†]

[1]Media Lab, Massachusetts Institute of Technology (MIT), Cambridge, MA, USA.

[2]MIT McGovern Institute for Brain Research, MIT, Cambridge, MA, USA.

[3]Department of Biomedical Engineering, Boston University, Boston, MA, USA.

[4]Stanley Center for Psychiatric Research, Broad Institute of MIT and Harvard, Cambridge, USA.

[5]Department of Mechanical and Industrial Engineering, University of Illinois, Chicago, USA.

[6]Howard Hughes Medical Institute, Department of Neurobiology, Harvard Medical School, Boston, MA, USA.

[7]Department of Biological Engineering, MIT, Cambridge, MA, USA.

[8]MIT Center for Neurobiological Engineering, MIT, Cambridge, MA, USA.

[9]Department of Brain and Cognitive Sciences, MIT, Cambridge, MA, USA.

[10]Koch Institute, MIT, Cambridge, MA, USA.

Abstract

A longstanding goal in neuroscience has been to image membrane voltage across a population of individual neurons in an awake, behaving mammal. Here, we report a genetically encoded fluorescent voltage indicator, SomArchon, which exhibits millisecond response times and compatibility with optogenetic control, and which increases the sensitivity, signal-to-noise ratio,

†co-corresponding authors; xuehan@bu.edu, esb@media.mit.edu.

Author Contributions

K.D.P. and E.S.B. initiated the project. K.D.P., S.B., H.T., S.N.S., X.H., and E.S.B. designed all *in vivo* experiments and interpreted the data. K.D.P. developed SomArchon and together with E.E.J., O.A.S., and E.C. characterized all constructs in cultured cells. K.D.P., V.G.L.H., D.P., C.S., and B.L.S. performed characterization of SomArchon in acute brain slices. S.B., S.N.S. and H.J.G. performed all mouse surgeries for *in vivo* experiments. M.F.R. assisted on imaging setups. K.D.P, S.B., H.T., and S.N.S performed all *in vivo* imaging experiments and analyzed all *in vivo* imaging data. K.D.P., S.B., H.T., S.N.S, X.H. and E.S.B. wrote the paper with contributions from all of the authors. E.S.B. and X.H. oversaw all aspects of the project. The funders had no role in study design, data collection and analysis, decision to publish, or preparation of the manuscript.

*These authors contributed equally: Kiryl D. Piatkevich, Seth Bensussen, and Hua-an Tseng.

Competing interests. The authors declare no competing financial interests.

Code availability. Computer codes used to generate results for this study are available at https://github.com/HanLabBU/somarchon-imaging.

Data availability. The data that support the findings of this study are available from the corresponding author upon reasonable request; raw data essential to the work is avalible online at nature.com. Sequences of the reported proteins are available at Genbank at the following accession codes: SomArchon MN091368; SomArchon-P2A-CoChR-$K_V2.1_{motif}$, MN091369.

and number of neurons observable, by several-fold over previously published reagents[1-8]. Under conventional one-photon microscopy, SomArchon enables population analysis of approximately a dozen neurons at once, in multiple brain regions: cortex, hippocampus, and striatum, of head-fixed, awake, behaving mice. Using SomArchon, we detected both positive and negative responses of striatal neurons during movement, previously reported by electrophysiology but not easily detected using modern calcium imaging techniques[9-11], highlighting the power of voltage imaging to reveal bidirectional modulation. We also examined how spikes relate to subthreshold theta oscillations of individual hippocampal neurons, with SomArchon reporting that individual neurons' spikes are more phase locked to their own subthreshold theta oscillations than to local field potential theta oscillations. Thus, SomArchon reports both spikes as well as subthreshold voltage dynamics in awake, behaving mice.

Near-infrared genetically encoded voltage indicators (GEVIs) derived from rhodopsins offer high temporal fidelity, and are compatible with optogenetics[1,12,13], whereas green fluorescent GEVIs derived from voltage sensing domains of phosphatases or opsins are often slower and brighter[2,3,14-17]. Translating these voltage sensors into the living mammalian brain has been challenging, because of poor membrane localization, photostability, and low signal-to-noise ratio (SNR). So far, only Ace2N and paQuasAr3-s have been used to optically report voltage dynamics in a living mouse brain, reporting the activities from up to four cells in one field of view (FOV) in awake mice[4,17]. Recently, we developed a robotic directed evolution approach and created the improved GEVI Archon1[13]. To further improve SNR in the dense, living mammalian brain, we conducted a screen for peptides to localize Archon1 to the soma[18-21], so that neuropil contamination could be reduced (Extended Data Fig. 1; see Supplementary Table 2 for the sequences of the motifs). The molecule Archon1-KGC-EGFP-K_V2.1-motif-ER2, which we call SomArchon (Fig. 1a), exhibited the highest ΔF/F during 100-mV voltage steps (Fig. 1g) and good soma localization (Extended Data Fig. 1h-k).

SomArchon fluorescently reported action potentials in mouse brain slice after *in utero* electroporation (IUE) into cortex and hippocampus, and after adeno-associated virus (AAV)-mediated expression in cortex, striatum, and thalamus (Extended Data Fig. 2). SomArchon was localized primarily to the membrane within 30–45 μm from the cell body in the cortex, striatum, and hippocampus (Fig. 1b; Extended Data Fig. 1h-k). SomArchon exhibited about two-fold greater sensitivity (Fig. 1c and d), and comparable kinetics (Fig. 1e) and signal to noise ratio (Fig. 1f, SNR, defined as the maximum fluorescence change observed during an action potential divided by the standard deviation of the baseline) to our previously published values for Archon1[13]. SomArchon linearly reported voltage (Fig. 1g), and did not alter membrane properties or resting potential in mouse brain slices, induce gliosis, or mediate light-induced phototoxicity (Extended Data Figs. 3, 4). We previously demonstrated that Archon1 exhibits no crosstalk under blue light illumination as used commonly for optogenetic neural activation[13]. We used a bicistronic expression system (Fig. 1h) to co-express SomArchon and the high-performance channelrhodopsin CoChR[22] in the same cell, and demonstrated that brief blue light pulses could reliably evoke action potentials visible in SomArchon fluorescence (Fig. 1i,j).

We performed a side-by-side comparison of SomArchon with soma-localized versions of several next-generation voltage sensors, specifically QuasAr3[4], paQuasAr3[4], ASAP3[5], and Voltron$_{525}$[6], in mouse cortical brain slice, focusing on layer 2/3 neurons, under identical expression conditions (Supplementary Table 3). The spectrally similar sensors QuasAr3, paQuasAr3, and SomArchon were recorded under identical imaging conditions (1.5W/mm^2), during CoChR-mediated action potentials. ASAP3 and Voltron were recorded with filter sets used in their respective preprints[5,6], under similar excitation intensities used in the Voltron pre-print [6] (25–29 mW/mm^2), during action potentials evoked upon application of 4-aminopyridine. Under these conditions, SomArchon exhibited the highest ΔF/F and SNR per action potential (Extended Data Fig. 5); in addition, SomArchon exhibited values higher than those previously reported for Ace2N-mNeon[7], ASAP1[2], MacQ-mCitrine[3], and QuasAr2[8] (see Supplementary Table 3 for details). In addition, SomArchon showed higher photostability than soma localized versions of ASAP3 and Voltron$_{525}$ under comparable imaging conditions in cultured neurons (Extended Fig. 5e).

We virally expressed SomArchon *in vivo* in the mouse motor cortex, visual cortex, striatum, and hippocampus, and imaged neural activity while mice were awake and head-fixed under a conventional one-photon microscope (Fig. 2a) using an sCMOS camera and laser excitation light at 637 nm, at a power of ~1.6 W/mm^2 (75mW; 20x objective lens), ~4 W/mm^2 (75mW; 40x objective lens), or ~1.6 W/mm^2 (95mW; 16x objective lens). SomArchon expressing cells could be resolved at depths ~50–150 μm below the imaging surface (Fig. 2b). We could detect individual spikes in single cells across all four brain regions (Fig. 2c, e, g, i, and Supplementary Video 1). The SNR per action potential ranged from ~7 to ~16 across the brain regions examined (Fig. 2d, f, h, j). No other paper reports SNR values per action potential in living mouse brain, so we cannot directly compare our molecule to others in this regard. We were able to resolve short segments of proximal dendrites next to the soma, and detected voltage fluctuation patterns that sometimes differed from those in the soma (Extended Fig. 6c-f). Additionally, simultaneous optical control and voltage imaging was feasible using the strategy of Fig. 1h, in awake behaving mice (Fig. 2k-m).

Electrophysiology has demonstrated that many striatal neurons increase their responses during movement[9,23], while others decrease their responses [9,10]. While electrophysiology recordings largely discard spatial information regarding the relative location of the neurons being observed, recent calcium imaging studies have revealed that spatially clustered striatal neurons are activated by similar aspects of movement[11]. These calcium imaging studies focused on the increases in activity during movement; decreases in activity are harder to observe with calcium imaging. We performed voltage imaging while mice ran on a spherical treadmill (Fig. 3a), identifying cell bodies and spikes from cells in the striatum (Fig. 3b-d), and aligned spiking activity to movement (Fig. 3d). Some neurons exhibited firing patterns known to occur in striatal fast spiking interneurons[24] or cholinergic interneurons[25] (Extended Fig. 7a-d). We found that 4 of the 14 neurons were positively modulated by movement speed, and 2 were negatively modulated by movement speed (Fig. 3e, f, Extended Data Fig. 7e,f; statistics in Supplementary Table 2). Furthermore, adjacent neurons did not respond to movement speed in identical ways. For example, in two recordings with three neurons each, we found that one of the three neurons was positively modulated by movement speed whereas the other two were not (Fig. 3f, Extended Data Fig. 7a,c; see Cells

1, 2, 3, and Cells 6, 7, 8; and Supplementary Table 2). Thus, SomArchon can readily detect decreases in striatal neuron spiking during movement, and help disambiguate activity changes amongst spatially clustered striatal neurons.

We performed wide-field voltage imaging with SomArchon in hippocampal CA1 neurons in awake, head-fixed mice, while simultaneously recording LFPs. *In vivo* patch clamp recordings have shown stronger phase-locking of a CA1 neuron's spikes to its own intracellular theta frequency (4–10Hz) oscillations, than to the across-neuron averaged LFP theta oscillations[26,27]. We found that 6 of the 16 neurons had spikes phase-locked to both intracellular and LFP theta oscillations (example in Fig. 4a), and 9 were phase locked only to intracellular theta oscillations, but not to LFP theta oscillations (example in Fig. 4b). As a population, neurons exhibited stronger phase locking to intracellular theta oscillations than to LFP theta oscillations (Fig. 4c,d). SomArchon thus supports the analysis of subthreshold intracellular oscillations, although interpretation of these measurements must take into account background fluorescence, which in densely labelled tissue may result in crosstalk that affects correlations.

We evaluated SomArchon photostability *in vivo*, and found a slight decrease in intensity in both the striatum and the hippocampus over time, but the SNR remained largely stable in both brain regions (Extended Data Fig. 8). In the hippocampus, firing rates remained constant over time, and we were able to continuously image for up to 80 seconds with minimal changes in SNR (Extended Data Fig. 8i-m, Supplementary Video 1). This lack of toxicity is consistent with our results from cultured neurons (Extended Data Fig. 3).

Due to the high performance and soma-targeted nature of SomArchon, we were able to routinely image multiple neurons at once in both cortical and subcortical brain regions (Figs. 2k,l, Fig. 3b,c, Extended Data Fig. 6a,b). In the hippocampus, using a 20x objective lens, we were able to record from 14 neurons at once, 8 of which were spiking (Fig. 4e,f). In addition, using a 16x objective lens, we routinely recorded from approximately a dozen cells at once (n = 13.1±3.5 neurons per FOV, mean±standard deviation, from 13 recording sessions in 2 awake mice). Of the 170 manually identified neurons, 107 (63%) spiked during the recording periods (duration: 13.5–27 seconds; Supplementary Table 4 and examples in Extended Data Fig. 6g-j). The ability to simultaneously record from multiple neurons allowed us to examine correlation and coherence of subthreshold activities between neuron pairs, though background fluorescence crosstalk between nearby neurons will need to be considered when interpreting pairwise correlation/coherence measurements (see Supplementary Discussion, Extended Data Figs. 9e-h, 10).

Compared to existing GEVIs, SomArchon achieves a severalfold improvement in the number of cells simultaneously imaged, while being fully genetically encoded and using inexpensive one-photon microscopy. The previously published record for fully genetically encoded voltage imaging was 4 spiking cells recorded simultaneously in an awake behaving mice, but requires a specialty imaging setup that combines two-photon structural imaging to support patterned single-photon excitation illumination targeting individual cell bodies, as well as the blue light-gated molecule paQuasAr3 that is incompatible with commonly used pulsed blue light optogenetic modulation[4]. ASAP3 has been used to image three dendrites at

once, with 2-photon microscopy, but this approach can only be used to record single cells at the fast rates typical for voltage imaging[5]. The hybrid GEVI sensor Voltron enables imaging of 46 neurons[6], but requires the addition of chemicals delivered to the living brain that complicate *in vivo* mammalian use, is not compatible with optogenetics, and exhibits lower dynamic range than SomArchon (Extended Data Fig. 5). Voltron, ASAP3, and Ace2N-mNeon all exhibit crosstalk with rhodopsins hampering their use with optogenetic actuators. Voltage imaging with SomArchon, as well as QuasAr3, is mainly limited by the high power and illumination spot of the 637 nm excitation laser; however, our data suggest that high powered 637 nm excitation does not induce more phototoxicity than with common, lower-powered 470 nm excitation (Extended Data Fig. 3). In conclusion, SomArchon is fully genetically encoded, compatible with conventional easily accessible one-photon widefield fluorescence microscopes, fully compatible with blue light-driven optogenetics, and enables routine imaging of a dozen neurons in a single FOV. We anticipate that the practicality of SomArchon will enable its rapid deployment into a diversity of contexts in neuroscience. As camera performance improves in years to come, and as further evolution of GEVIs continues, we anticipate that perhaps dozens to hundreds of neurons will be imageable with simple one-photon optics in the near future.

Methods

Molecular cloning.

For screening candidates for the soma-localized Archon1 voltage sensor in primary hippocampal neurons, DNA encoding for candidate localization motifs were synthesized *de novo* with mammalian codon optimization and subcloned with Archon1 (GenBank ID MG250280.1) and EGFP genes into the pAAV-CAG vector to obtain the final constructs described in Supplementary Table 1 (gene synthesis and subcloning were performed by Epoch Life Science Inc.). For *in vivo* expression in the mouse brain via *in utero* electroporation (IUE), the Archon1-KGC-EGFP-$K_V2.1_{motif}$-ER2, QuasAr3-PP-Citrine-$K_V2.1_{motif}$-ER2 (QuasAr3-s), paQuasAr3-PP-Citrine-$K_V2.1_{motif}$-ER2 (paQuasAr3-s) and CoChR-mTagBFP2-$K_V2.2_{motif}$-ER2 genes were subcloned into the pCAG-WPRE vector. The QuasAr3-PP-Citrine-K_V2.1-ER2 and paQuasAr3-PP-Citrine-K_V2.1-ER2 gene were synthesized de novo (GenScript Biotech Corp.) based on sequences reported in the original preprint[28]. The CoChR-mTagBFP2-$K_V2.2_{motif}$-ER2 gene was assembled by Epoch Life Science Inc. using pAAV-Syn-CoChR-GFP (Addgene plasmid #59070) and pBAD-mTagBFP2 (Addgene plasmid #34632) as the source of the CoChR and mTagBFP2 genes, respectively; the K_V2.2 motifs were synthesized *de novo* with mammalian codon optimization (Epoch Life Science Inc.). The pAAV-Syn-Archon1-KGC-EGFP-$K_V2.1_{motif}$-P2A-CoChR-$K_V2.1_{motif}$ plasmid was also cloned by Epoch Life Science Inc. We used the Kv2.1motif fused to CoChR for the following reason: in our original paper on soma-targeted CoChR[18], we used the KA2 sequence, which worked best with CoChR-GFP, but in this paper we used fluorophore-free CoChR, which did not express well with KA2, and rather worked better with K_V2.1; we also sometimes used the corresponding sequence from K_V2.2 as described in the text. Plasmid amplification was performed using Stellar (Clontech Laboratories Inc.) or NEB10-beta (New England BioLabs Inc.) chemically competent *E. coli* cells. Small-scale isolation of plasmid DNA was performed with Mini-Prep kits (Qiagen);

large-scale DNA plasmid purification was done with GenElute HP Endotoxin-Free Plasmid Maxiprep Kits (Sigma-Aldrich Corp.). The ASAP3-Kv and Voltron-ST genes were synthesized *de novo* by GenScript, based on the sequences reported in the corresponding pre-prints[5,6], and cloned into pCAG-WPRE vector.

Neuronal culture and transfection.

All mouse procedures were performed in accordance with the National Institute of Health Guide for Laboratory Animals and approved by the Massachusetts Institute of Technology Institutional Animal Care and Use and Biosafety Committees. For dissociated hippocampal mouse neuron culture preparation, postnatal day 0 or 1 Swiss Webster mice without regard to sex (Taconic Biosciences Inc., Albany, NY) were used as previously described[13]. Briefly, dissected hippocampal tissue was digested with 50 units of papain (Worthington Biochemical Corporation) for 6–8 min at 37 °C, and the digestion was stopped by incubating with ovomucoid trypsin inhibitor (Worthington Biochemical Corporation) for 4 min at 37 °C. Tissue was then gently dissociated with Pasteur pipettes, and dissociated neurons were plated at a density of 20,000–30,000 per glass coverslip coated with Matrigel (BD Biosciences). Neurons were seeded in 100 μL plating medium containing MEM (Life Technologies Corp.), glucose (33 mM, Sigma), transferrin (0.01%, Sigma), Hepes (10mM, Sigma), Glutagro (2 mM, Corning), Insulin (0.13%, Millipore), B27 supplement (2%, Gibco), and heat inactivated FBS (7.5%, Corning). After cell adhesion, additional plating medium was added. AraC (0.002 mM, Sigma) was added when glia density was 50–70% of confluence. Neurons were grown at 37°C and 5% CO2 in a humidified atmosphere.

For *in vitro* screening of candidate soma-localized Archon1 sensors, primary hippocampal neuron cultures were transfected with 500 ng of plasmid DNA per well with a commercial calcium phosphate transfection kit (Life Technologies Corp.) after 4 days *in vitro* (DIV), as previously described. After 30–60 min of DNA-calcium phosphate precipitate incubation with cultured neurons at 37°C, neurons were washed twice with acidic MEM buffer (pH 6.7–6.8) to remove residual calcium phosphate particles and returned to the original plating media. All measurements on cultured neurons were taken between days in vitro (DIV) 14 and DIV 18 (~9–14 d post transfection) to allow for sodium channel maturation (and thus spiking). No all-trans-retinal was supplemented for any cultured neuron recordings.

Electrophysiology and fluorescence microscopy in cultured primary hippocampal neurons.

Whole-cell patch clamp recordings of cultured neurons for Supplementary Table 1 were acquired via an Axopatch 700B amplifier (Molecular Devices LLC) and Digidata 1440 digitizer (Molecular Devices LLC). Neurons were patched between DIV14 and DIV18 and were bathed in Tyrode's solution (125mM NaCl, 2mM KCl, 3mM CaCl2, 1mM MgCl2, 10mM HEPES, 30mM glucose, pH 7.3 (NaOH adjusted)) at 32 °C during measurements. Synaptic blockers (NBQX, 10μM; d(–)-2-amino-5-phosphonovaleric acid, 25 μM; gabazine, 20μM; Tocris) were added to the extracellular solution for single-cell electrophysiology. Borosilicate glass pipettes with an outer diameter of 1mm and a wall thickness of 0.2mm were pulled to produce electrodes with resistance of 3–10 MΩ and were filled with an internal solution containing 135mM potassium gluconate, 8mM NaCl, 10mM HEPES, 4mM

Mg-ATP, 0.4mM Na-GTP, 0.6mM MgCl2, 0.1mM CaCl2, pH 7.25 (KOH adjusted) at 295mOsm. Measurements from primary neuron cultures were performed on the electrophysiology setup described above. Patch-clamp data was acquired only if the resting potential was below −45mV and access resistance was <25 MΩ. Access resistance was compensated at 30–70%. Fluorescence imaging was performed on an inverted fluorescence microscope (Nikon Ti), equipped with a red laser (637 nm, 100 mW, Coherent, OBIS 637LX, Pigtailed) expanded by a beam expander (Thorlabs Inc) and focused onto the back focal plane of a 40×NA 1.15 objective lens (Nikon Corp.).

Two-photon imaging of SomArchon expressing neurons was performed using an Olympus FVMPE-RS equipped with two lasers for fluorescence excitation. An InSight X3 laser (Spectra-Physics) tuned to 1150 nm at 50% transmissivity was used to excite SomArchon, and a MaiTai HP Ti:Sapphire laser (Spectra-Physics) tuned to 920 nm at 15% transmissivity was used to excite EGFP. The laser beams were focused by a 25× 1.05 NA water-immersion objective lens (Olympus). SomArchon emission was separated using a 590 nm dichroic mirror and imaged with 660–750 nm and 495–540 nm filters for near-infrared and green fluorescence, respectively, and signals were collected onto separate photomultiplier tubes. Imaging was performed at 2.0 μs/pixel sampling speed with one-way galvano scanning.

Phototoxicity and photobleaching measurements in cultured neurons.

For phototoxicity and photostability measurements, primary mouse neuron cultures, prepared as described above, were imaged using an inverted Eclipse Ti-E microscope (Nikon) equipped with a sCMOS camera (OrcaFlash4.2, Hamamatsu), LED light source (Spectra, Lumencor), a 637 nm Laser (637 LX, OBIS) focused on the back focal plane of a 40× NA 1.15 water immersion objective lens (Nikon), and a Polygon400 Multi-wavelength Patterned Illuminator (Mightex) with a 470 nm LED (ThorLabs). To express SomArchon, neurons were infected with AAV2-CaMKII-SomArchon or AAV2-Syn-SomArchon-P2A-CoChR-$K_V2.1_{motif}$ at DIV 5. To express ASAP3-Kv and Voltron-ST, neurons were transfected with the pCAG-ASAP3-Kv-WPRE and pCAG-Voltron-ST-WPRE plasmids, respectively, using the calcium phosphate method described above. For imaging of Voltron-expressing neurons, the cells were incubated with JF525 at final concentration 1.25 μM for 60 min at 37°C (application of higher concentration of JF525 resulted in significant internalization of the dye with 40 min of incubation at 37°C thus completely preventing functional imaging due to high background fluorescence). After incubation, the cells were washed 3 times with fresh plating media for 3 h to removed unbound dye. The ROS measurements were performed using CellRox Orange dye (Invitrogen) according to the manufacturer's protocol. Briefly, neurons were incubated with the CellROX Orange reagent at a final concentration of 5 μM for 30 minutes at 37°C in darkness, and then washed once with fresh plating media prior to imaging. Right before imaging, cells were supplemented with the NucGreen Dead 488 reagent for detection of the plasma membrane integrity, which we used to indicate cell death. Cells that showed a >10 times increase in green fluorescence in the nucleus over background fluorescence levels were considered dead. Neurons were imaged between DIV 14 and DIV 18 in the plating media at 22°C. CellROX Orange fluorescence was acquired using 510/25 nm excitation at 0.8 mW/mm^2 and 545/40 nm

emission. NucGreen fluorescence was acquired using 475/36 nm excitation at 3.5 mW/mm^2 and 527/50 nm emission.

In utero electroporation, AAV injection, and acute brain slice preparation.

For IUE, embryonic day (E) 15.5 timed-pregnant female Swiss Webster (Taconic Biosciences Inc., Albany, NY) mice were deeply anesthetized with 2% isoflurane. Uterine horns were exposed and periodically rinsed with warm sterile PBS. Plasmid DNA (1–2 μg total at a final concentration of ~2–3 μg/μL diluted in sterile PBS) was injected into the lateral ventricle of one cerebral hemisphere of an embryo. Five voltage pulses (50 V, 50 ms duration, 1 Hz) were delivered using 5 mm round plate electrodes (ECM™ 830 electroporator, Harvard Apparatus), placing anode or cathode on the top of the skull to target cortex or hippocampus, respectively. Electroporated embryos were placed back into the dam, and allowed to mature to delivery. Brain slices were prepared from electroporated mice without regard to sex at P12-P22.

The electroporated mice were anaesthetized by isoflurane inhalation, decapitated, and cerebral hemispheres were quickly removed and placed in cold choline-based cutting solution consisting of (in mM): 110 choline chloride, 25 NaHCO3, 2.5 KCl, 7 MgCl2, 0.5 CaCl2, 1.25 NaH2PO4, 25 glucose, 11.6 ascorbic acid, and 3.1 pyruvic acid (339–341 mOsm/kg; pH 7.75 adjusted with NaOH) for 2 min, then blocked and transferred into a slicing chamber containing ice-cold choline-based cutting solution. For mice electroporated with Voltron-ST, 50 μL of JF525 dye (Janelia Farm; 12.5 nM of JF525 in 10μL of DMSO mixed with 10 μL Pluronic F-127 (20% w/v in DMSO; Invitrogen) and 30 μL of sterile PBS) was injected into the retro-orbital sinus one day before slicing. Coronal slices (300 μm thick) were cut with a Compresstome VF-300 slicing machine, then transferred to a holding chamber with artificial cerebrospinal fluid (ACSF) containing (in mM) 125 NaCl, 2.5 KCl, 25 NaHCO3, 2 CaCl2, 1 MgCl2, 1.25 NaH2PO4 and 11 glucose (300–310 mOsm/kg; pH 7.35 adjusted with NaOH), and recovered for 10 min at 34 °C, followed by another 30 min at room temperature. Slices were subsequently maintained at room temperature (22^{o}C) until use. Both cutting solution and ACSF were constantly bubbled with 95% O2 and 5% CO2.

For AAV injection, 21-day-old C57 BL/6J mice were anesthetized with isoflurane and placed in a small animal stereotaxic apparatus (David Kopf Instruments, CA, USA). Animals were injected with a volume of 200 nl rAAV8-Syn-Archon1-KGC-EGFP-Kv2.1motif-ER2 using a Nanoject (Drummond Scientific Co Inc, Broomall, PA) via glass pipettes with 20–30 μm diameter tips in striatum: anteroposterior (AP) 1.2, mediolateral (ML) 2.1, dorsoventral (DV) 3.2. Brain slices were then prepared from these AAV-injected mice at postnatal day 30–35. Mice were deeply anesthetized with isoflurane and perfused transcardially using cold saline containing (in mM): 194 sucrose, 30 NaCl, 4.5 KCl, 1.2 NaH_2PO_4, 0.2 $CaCl_2$, 2 $MgCl_2$, 26 $NaHCO_3$, and 10 D-(+)-glucose saturated with 95% O_2 and 5% CO_2, pH=7.4 adjusted with NaOH, 320–340 mOsm/L. Coronal slices (250–300 μm thick) were cut using a slicer (VT1200 S, Leica Microsystems, USA) and then incubated for 10 – 15 min in a holding chamber (BSK4, Scientific System Design Inc., USA) at 32°C with regular ACSF containing (in mM): 136 NaCl, 3.5 KCl, 1 $MgCl_2$, 2.5 $CaCl_2$, 26 $NaHCO_3$

and 11 glucose saturated with 95% O_2 and 5% CO_2, followed by at least one hour recovery at room temperature (21–25°C) before recording.

Concurrent electrophysiology and fluorescence imaging in acute brain slice.

For recording in Figure 1 and Extended Data Fig. 3a-c, individual slices were transferred to a recording chamber mounted on an upright microscope (Olympus BX51WI, see below) and continuously superfused (2–3 mL/min) with carbogenated ACSF at room temperature. Whole cell patch-clamp recordings were performed with borosilicate glass pipettes (KG33, King Precision Glass Inc.) heat polished to obtain direct current resistances of ~4–6 MΩ. For cortex recordings, pipettes were filled with an internal solution containing in mM: 120 K-Gluconate, 2 MgCl2, 10 HEPES, 0.5 EGTA, 0.2 Na2ATP, and 0.2 Na3GTP. For hippocampus and striatum recordings, pipettes were filled with an internal solution containing in mM: 131 K-Gluconate, 17.5 KCl, 9 NaCl, 1 MgCl2, 10 HEPES, 1.1 EGTA, 2 Na2ATP, and 0.2 Na3GTP. Voltage clamp recordings were made with a microelectrode amplifier (Multiclamp 700B, Molecular Devices LLC). Cell membrane potential was held at −60 mV, unless specified otherwise. Signals were low-pass filtered at 2 kHz and sampled at 10–20 kHz with a Digidata 1440A (Molecular Devices LLC), and data were stored on a computer for subsequent off-line analysis. Cells in which the series resistance (Rs, typically 8–12 MΩ) changed by >20% were excluded from subsequent data analysis. In addition, cells with Rs more than 25 MΩ at any time during the recordings were discarded. In some cases, conventional characterization of neurons was made in both voltage and current clamp configurations. Positive neurons were identified for recordings on the basis of EGFP expression visualized with a microscope equipped with a standard GFP filter (BX-51WI, Olympus Corp.). Optical voltage recordings were taken through a 40x water immersion objective (Olympus LUMFL N 40x/0.8W). Fluorescence was excited using a fiber-coupled 637 nm red laser (140mW, Coherent Obis 637–140 LX), and the emission was filtered through a 664 long pass filter. Images were collected on an EMCCD camera (Andor iXON Ultra 888) or sCMOS camera (Andor Zyla4.2 Plus Andor) in a reduced pixel window to enable acquisition at ~1kHz. Each trial was about 30 seconds in duration. Of the 18 cortical neurons reported in Figure 1, four neurons were not analyzed for Figure 1e because the electrophysiology files were inadvertently not saved, owing to manual save process clunkiness.

For optical recordings in Figure 1i, j and Extended Data Figs. 1a-g, 2, 5, acute brain slices were transferred to a recording chamber mounted on an inverted Eclipse Ti-E (Nikon) equipped with a CMOS camera (Zyla5.5, Andor), LEDs (Spectra, Lumencor), a 637nm Laser (637 LX, OBIS) focused on the back focal plane of a 40×NA 1.15 objective (Nikon), and a Polygon400 Multiwavelength Patterned Illuminator (Mightex) with 470 nm LED (ThorLabs), and continuously superfused (2–3 mL/min) with carbogenated ACSF at room temperature. Positive cells were imaged under 0.8 or 1.5 W/mm^2 (55 mW) excitation light power at 637 nm from the laser. 4-aminopyridine at a final concentration of 1 mM was added to induce neuronal activity for experiments in Extended Data Fig. 2c,d,g,h, 5. For Figure 1i, j and Extended Data Fig. 5, cells were illuminated with 2 ms blue light pulses at light power in the range from 0.1 to 1.0 mW/mm^2.

Mouse surgery.

All *in vivo* mouse procedures were performed in accordance with the National Institute of Health Guide for Laboratory Animals and approved by the Boston University Institutional Animal Care and Use and Biosafety Committees.

Virus injection surgery: All AAV was produced by the University of North Carolina Chapel Hill Vector Core. Adult female C57BL/6 mice (Charles River Laboratories, Inc.) or Chat-Cre mice (Chat-cre;129S6-Chattm2(cre)Lowl/J, the Jackson Laboratory), 8–12 weeks at the time of surgery, were used for all experiments. AAV-Syn-SomArchon (5.9e12 genome copies (GC)/ml) or AAV-syn-SomArchon-P2A-CoChR-Kv2.1 (2.19e13 GC/ml) was injected into the motor cortex (AP: +1.5, ML: +/−1.5, DV: −0.3, 0.5uL virus), visual cortex (AP: −3.6, ML: +/−2.5, DV: −0.3, 0.5uL virus), hippocampus (AP:−2.0, ML:+1.4, DV:−1.6, 1uL virus) or striatum (AP:+0.8, ML:−1.8, DV:−2.1, 1uL virus). Viral injection occurred at 50–100nL/min (ten minutes total) using a 10uL syringe (NANOFIL, World Precision Instruments LLC) fitted with a 33 gauge needle (World Precision Instruments LLC, NF33BL) and controlled by a microinfusion pump (World Precision Instruments LLC, UltraMicroPump3–4). The syringe was left in place for an additional 10 minutes following injection to facilitate viral spread. About one week following the viral injection, mice underwent a second surgery to implant the cranial window for *in vivo* imaging.

Cortex imaging window implantation.—The imaging window consisted of a stainless steel cannula (OD: 3.17mm, ID: 2.36mm, 1mm height, AmazonSupply, B004TUE45E) fitted with a circular coverslip (#0, OD: 3mm, Deckgläser Cover Glasses, Warner Instruments LLC, 64–0726 (CS-3R-0)) adhered using a UV curable glue (Norland Products Inc., Norland Optical Adhesive 60, P/N 6001). A craniotomy of ~3mm in diameter was created, with the dura left intact, over the motor cortex (centered at AP: +1.5, ML: +/−1.75) or visual cortex (AP: −3.6, ML: +/− 2.15). The imaging window was positioned over the cortex so that it was flush with the dura surface. Kwik sil adhesive (World Precision Instruments LLC, KWIK-SIL) was applied around the edges of the imaging window to hold the imaging window in place and to prevent any dental cement from touching the brain. Three small screws (J.I. Morris Co., F000CE094) were screwed into the skull to further anchor the imaging window to the skull. Dental cement was then gently applied to affix the imaging window to the exposed skull, and to mount an aluminum headbar posterior to the imaging window. See Supplementary Methods Fig. 1a,b for window placement.

Hippocampus and striatum imaging window implantation.—Hippocampal and striatal window surgeries were performed similar to those described previously[11,29]. For each imaging window, a virus/drug infusion cannula (26G, PlasticsOne Inc., C135GS-4/SPC) was attached to a stainless steel imaging cannula (OD: 3.17mm, ID: 2.36mm, 1 or 2mm height, AmazonSupply, B004TUE45E). The bottom of the infusion cannula was flush with the base of the stainless steel cannula, and a circular coverslip (#0, OD: 3mm, Deckgläser Cover Glasses, Warner Instruments Inc., 64–0726 (CS-3R-0)) was adhered using a UV curable glue (Norland Products Inc., Norland Optical Adhesive 60, P/N 6001). An additional insulated stainless steel wire (Diameter: 130μm, PlasticsOne Inc., 005SW-30S, 7N003736501F) was glued to the viral/drug infusion cannula with super glue (Henkel Corp.,

Loctite 414 and Loctite 713) and protruded from the bottom of the infusion cannula and imaging window by about 200μm for LFP recordings.

A craniotomy ~3mm in diameter was made over the hippocampus CA1 region (AP: −2.0, ML: +2.0) or the striatum (AP: +0.8, ML: −1.8). A small notch was made on the posterior edge of the craniotomy to accommodate the infusion cannula and LFP recording electrode. The overlying cortex was gently aspirated using the corpus callosum as a landmark. The corpus callosum was then carefully thinned in order to expose the hippocampus CA1 region or the dorsal striatum. The imaging window was positioned in the craniotomy, and Kwik sil adhesive (World Precision Instruments LLC, KWIK-SIL) was applied around the edges of the imaging window to hold it in place and to prevent any dental cement from touching the brain. Three small screws (J.I. Morris Co., F000CE094) were screwed into the skull to further anchor the imaging window to the skull, and a small ground pin was inserted into the posterior part of the brain near the lambda suture as a ground reference for LFP recordings. Dental cement was then gently applied to affix the imaging window to the exposed skull, and to mount an aluminum headbar posterior to the imaging window. See Supplementary Methods Fig. 1c,d for window placement.

In mice that did not receive a virus injection prior to window implantation, 1uL of AAV-syn-SomArchon (5.9e12 GC/ml) or 1uL of AAV-syn-SomArchon-P2A-CoChR-Kv2.1 (2.19e13 GC/ml), or 1μL of AAV-CAG-FLEX-SomArchon (6.3e12 GC/ml) was injected through the virus/drug infusion cannula at 100nL/min through an internal infusion cannula (33G, PlasticsOne Inc., C315IS-4/SPC) connected to a microinfusion pump (World Precision Instruments LLC, UltraMicroPump3–4), one week after the window implantation surgery. The internal infusion cannula was left in place for 10 minutes following injection to facilitate viral spread. Mice were awake and head-fixed throughout the injection period.

All mice were treated with buprenex for 48 hours following surgery and single-housed to prevent any damage to the headbar or window implant.

In vivo imaging in the live mouse brain.

All optical recordings were acquired on a conventional one-photon fluorescence microscope equipped with an ORCA Flash 4.0 V3 Digital CMOS camera (Hamamatsu Photonics K.K., C13440–20CU) or Hamamatsu ORCA Fusion Digital CMOS camera (Hamamatsu Photonics K.K., C14440–20UP), 10x NA0.25 LMPlanFI air objective (Olympus Corp.), 40x NA0.8 LUMPlanFI/IR water immersion objective (Olympus Corp.), 20x NA1.0 XLUMPlanFL N water immersion objective (Olympus Corp.), 16x NA0.8 CFI LWD Plan Fluorite water immersion objective (Nikon), 470 nm LED (ThorLabs Inc., M470L3), 140 mW 637 nm red laser (Coherent Obis 637–140X), a green filter set with a 470/25 nm bandpass excitation filter, a 495 nm dichroic, and a 525/50 nm bandpass emission filter, and a near infrared filter set with a 635 nm laser dichroic filter, and a 664 nm long pass emission filter. The near-infrared laser illuminated a circular area of ~60–80 μm, ~80–140 μm, and ~100–200 μm in diameter in brain tissue, with FOV height (limited by camera acquisition rate) 40–60 μm, 80–100 μm, and 100–120 μm under 40x, 20x, and 16x objective lenses, respectively, and a mechanical shutter (Newport Corporation, model 76995) was positioned in the laser path to control the timing of illumination over the imaging window. Optical

recordings were acquired at 390–900 Hz with HCImage Live (Hamamatsu Photonics K.K.) or NIS Elements (Nikon) software. HC Image Live data were stored as DCAM image files (DCIMG), and further analyzed offline in Fiji/ImageJ and MATLAB (Mathworks Inc.). NIS Elements data were stored as .nd2 files and further analyzed offline using the NIS Elements software.

The GFP signal of SomArchon was acquired in the green channel (λ_{ex}=470 nm) at 1024×1024 pixels with 2×2 binning to show cell structure and distribution. Optical voltage recordings were imaged in the near infrared channel (λ_{ex}=637 nm) with 2×2 or 4×4 binning. OmniPlex system (PLEXON Inc.) was used to synchronize data acquisition from different systems. In all experiments, the OmniPlex system recorded the start of image acquisition from the sCMOS camera, the acquisition time of each frame, and other experiment-dependent signals described below.

Optical imaging of spontaneous neural activity.—All *in vivo* optical imaging of spontaneous neural activity was performed when mice were awake and head fixed in a custom holder that allowed for attachment of the headplate at the anterior end. Animals were covered with an elastic wrap to prevent upward movement. Spontaneous neural activity recordings lasted continuously up to 30,000 frames (~36 seconds).

Eye puff.—During some *in vivo* hippocampal imaging recordings, an eye puff was applied to evoke high frequency local field potential responses in the hippocampus (Extended Data Fig. 9a-d). The mice were head fixed in a custom holder that allowed for attachment of the headplate at the anterior end, and they were covered with an elastic wrap to prevent upward movement. Each experimental session consisted of 20–30 trials, with each trial lasting for 5000 frames (~6 seconds). Three seconds after the start of image acquisition, the sCMOS camera sent a TTL pulse to a function generator (Agilent Technologies, model 33210A), which triggered a 100ms long air puff. The air puff was 5–10 psi, and administered via a 0.5mm cannula placed 2–3cm away from the mouse's eye. The puff TTL pulses were also recorded with the OmniPlex system (PLEXON Inc.). Eye movement was monitored using a USB webcam (Logitech, Carl Zeiss Tessar 2.0/3.7 2MP Autofocus).

Optopatch blue light stimulation.—All *in vivo* optopatch (i.e., optogenetics plus voltage imaging) experiments were performed when mice were awake and head fixed in a custom holder that allowed for attachment of the headplate at the anterior end. Animals were covered with an elastic wrap to prevent upward movement. A 470nm LED (ThorLabs Inc., M470L3) was coupled to a Polygon400 Multiwavelength Patterned Illuminator (Mightex), and the blue light was focused through the objective lens to illuminate the center of the FOV. At the onset of imaging, the sCMOS camera sent a TTL pulse to trigger Axon CNS (Molecular Devices LLC, Digidata 1440A) which controlled the 470 nm LED (ThorLabs). Each trial lasted 1.1 second and consisted of a single 100 ms long blue light pulse, 500 ms after trial onset. Each recording session consisted of 10 trials with increasing blue light power from 0.1 to 1 mW/mm^2, with a step of ~ 0.1 mW/mm^2 per trial. The OmniPlex system (PLEXON Inc.) recorded the timing of TTL pulses used to trigger the Axon CNS.

Head-fixed voluntary movement experiments.—All voluntary movement experiments were performed while awake, head-fixed mice were freely navigating a spherical treadmill. The spherical treadmill was constructed following the design of [30]. Briefly, a 3D spherical Styrofoam ball was supported by air, and motion was tracked using two computer mouse sensors positioned roughly +/− 45 degrees from center along the equator of the ball. All motion sensor displacement data was acquired at 100 Hz on a separate computer and synthesized using a custom Python script. Motion sensor displacement data were then sent to the image acquisition computer to be accumulated using a modified ViRMEn MATLAB script. The timing of each motion sensor displacement data point was also recorded using the OmniPlex system (PLEXON Inc.) to synchronize movement data with optical voltage recordings.

In order to determine the mouse movement speed, ball movement was first calibrated. The ball was pinned on the two sides and rotated vertically to calibrate sensor displacement.

All mice were habituated on the spherical treadmill for at least three days, at least 20 minutes per day, prior to image acquisition. During optical imaging, mice were imaged while freely navigating the spherical treadmill. Each FOV was recorded for at least 36 seconds total. In some fields of view, we performed multiple trials, and each trial was at least 12 seconds in duration with an inter-trial interval of at least 30 seconds in duration.

Local field potential recording.

Local field potentials were recorded using an OmniPlex system (PLEXON Inc.) at a 1 kHz sampling rate. To synchronize optical recordings with LFP recordings, the camera sent out a TTL pulse to the OmniPlex system at the onset of imaging and after each acquired frame.

Motion correction.

In Figures 2i, 3, and 4, motion correction was performed with a custom Python script. For FOV, if multiple video imaging files were collected for the same FOV, we started with the first imaging file to ensure speedy data processing (a single video file contains a series of images). We first generated the reference image by averaging across all images within the file. We then performed a series of image processing procedures to enhance the contrast of the reference image and every image in the file to facilitate motion correction. We first removed 10% of the pixels along all edges of an image to remove any camera induced artifact. We then applied a high-pass filter (Python scipy package, ndimage.gaussian_filter, sigma=50) to remove low frequency components within the images. To enhance the boundary of high intensity areas, we identified the boundary as the difference between two low pass filtered images (sigma=2 and 1). We then enhanced the boundary by adding 100 times the boundary back to the low pass filtered image (sigma=2). We then limited the intensity range of the processed images within one standard deviation above and below the average intensity of the image, by setting the pixels with intensity higher than mean+std as mean+std, and the pixels with intensity lower than mean-std as zeroes. Finally, to counter any potential bleaching over time, we normalized the intensity of each image by shifting the mean intensity to zero and divided intensity values by the standard deviation of all pixel intensities in that image. After image processing, we calculated the displacement of each

image, by identifying the max cross-correlation coefficient between each image and the reference image, and then corrected motion by shifting the displacement in the original, unenhanced image sequence. If the same FOV was imaged over an extended period of time, where multiple files were acquired, we motion-corrected subsequent files by aligning them to the first file, so that the same ROIs from the same FOV could be applied across the entire imaging session. Specifically, we first refined the reference frame by generating the mean intensity projection image from the motion-corrected first imaging file. The refined reference image was then used to motion-correct all files of the same FOV, including the first file, using the same procedure described above. The motion-corrected, original, unenhanced image sequences, were then used for subsequent manual ROI segmentation, and further analysis.

ROI identification.

We imported the image files (motion-corrected as above, if necessary) into Fiji/ImageJ or NIS Elements and manually segmented ROIs by examining the time-series images to identify the area with clear neuron outlines and/or intensity dynamics over time. The optically-recorded voltage traces for each ROI were generated from the motion-corrected image sequences using the "multiple measurement" function and were then used for analyses.

The wide dynamic range (16 bit) of the raw images meant that to select dim as well as bright cells, we had to create max projection and standard deviation images of the entire raw video and stretched their LUTs (look up tables) to enhance visibility. For Figure 4 and Extended Data Fig. 9e-h, cells were densely packed, so we identified and tracked ROIs semi-manually across image sequences without performing motion correction. We first visually inspected all image sequences and identified those with minimal motion and with an SNR greater than ~2 for further analysis. We then performed an iterative ROI-selection procedure to identify ROIs that best fit each cell. Specifically, we started by manually selecting ROIs from the max projection image of the entire image sequence. The image sequence was then visually inspected to identify frames whose cells exhibited shifts of more than three pixels from the defined ROI. We then used these frames to separate the image sequence into multiple time intervals, and obtained a new set of max projection images to identify new ROIs within these time intervals for these cells. This procedure was repeated iteratively until the ROI represented the cell across all image frames in their corresponding time intervals without the cell moving out of the ROI. Thus, with this procedure, we created multiple ROIs representing the same cell across different frames. For each cell, we extracted traces for every ROI during its corresponding time interval, and stitched the baseline-normalized traces for the same cell(s) in time. The fluorescence traces of each cell were then detrended for further analysis. See Supplementary Methods Fig. 2 for an example of raw and processed traces for two cells in the same FOV.

Hippocampal spike detection.

Spikes were associated with a rapid increase in intensity, followed by a rapid decrease. In contrast, occasional motion artifacts were usually associated with a decrease in intensity as a neuron moved out of the ROI. To facilitate spike detection, we first removed motion

artifacts. For each time point of the fluorescence intensity trace for each ROI, we calculated the change in intensity from that of the prior time point (I_{change}). We then defined noise as the time points where instantaneous I_{change} were three standard deviations below the mean value of I_{change} across the entire trace. We excluded any time points where the I_{change} of the previous time point was more than one standard deviation above the average I_{change}, because this might have indicated a spike. These noise time points and their following three time points (since we found that motion artifacts are typically >4ms) were then considered motion artifacts, and removed from further analysis. We then recalculated the standard deviation of the I_{change}, excluding the data points of motion artifact. The peaks of spikes were then identified as time points with the following two criteria: 1) the intensity change of the time point combined with that of its preceding time point was more than three standard deviations above the average I_{change}, and 2) the intensity change over the next two time points was less than two standard deviations below the average I_{change}.

Hippocampal spike phase calculation.

Hippocampal spike-phase analysis was performed on 16 neurons from 7 FOVs from 4 mice. For each FOV, we analyzed data collected over 10 trials (~60 seconds total), where animals experienced an eye puff in each trial as described above in *Eye puff*. To calculate the phase of spikes at theta frequency (4–10 Hz), we first band-pass filtered both the optical voltage trace and the simultaneously recorded LFP at theta frequency (eegfilt, EEGLAB toolbox). The peaks of theta oscillation power were then identified with the findspike function in MATLAB. For each spike, we obtained the phase of the spike by calculating the timing of each spike relative to the period of that oscillation cycle in degrees. We averaged the phases of all spikes from the same neuron as the average phase of a given neuron.

Analysis for pair-wise coherence between hippocampal neurons and LFPs.

The coherence analysis was performed on 9 FOVs that contained multiple neurons from 4 mice. Each FOV contained imaging data over a period of 6–36 seconds. For each FOV, we first re-sampled the LFP at the acquisition rate of the optical imaging. We then divided the optical voltage traces and LFPs into segments of 1000 data points. We then calculated the averaged coherence, at theta frequency (4–10 Hz), with the functions in the Chronux toolbox (optical voltage trace to optical voltage trace or LFP: coherencyc, and spike to spike: coherencypt) with tapers=[10 19], fpass=[4 10] and trialave=1. To compare V_{mo}-V_{mo} coherence vs. V_{mo}-LFP coherence across nine FOVs, we averaged the coherence of neurons in the same FOV to obtain the mean coherence of that FOV, and then performed statistical tests across FOVs using the individual FOV's mean coherences. To understand the relationships between pairs of coherence, we used the MATLAB function, fitlm, to perform a linear regression between coherent pairs and obtain the p-value and r^2 value.

To estimate background fluorescence crosstalk, we calculated pair-wise coherence and correlation between background donut areas surrounding a neuron. To select background donut areas, we excluded the edges (5%) of each FOV, since the edge may be missing for a particular image frame when image frames were shifted during motion correction. The background donut of a neuron was determined as the area 3–10um from the neuron boundary, excluding any pixels within 10 um of the boundary of another neuron. One neuron

was excluded from this analysis due to dense labelling where we cannot identify its donut area. Fluorescence traces of the background donut area were then processed as that for neurons, and their pair-wise coherence and Pearson correlations were calculated.

Striatum, motor cortex, and visual cortex, spike detection.

After motion correction, we first identified large fluorescence increases using a threshold of 4 standard deviations above the baseline. The baseline was manually selected as a period of >500ms without spiking or drifting due to z-plane shifting or photobleaching. From these large fluorescence increases, we selected those with shorter than 4 ms rise times and 4 ms decay times as spikes.

Firing rate comparison of striatal neurons during high versus low speed movement.

Animals' movement data was first interpolated to the voltage imaging frame rate with MATLAB function interp1, and then smoothed using a 1.5Hz low pass Butterworth filter to remove any motion sensor artifact. We calculated the average movement speed at 0.5-second intervals and defined low speed periods as intervals where the average speed was $\leq$5cm/s and high speed periods as intervals where the average speed was $\geq$10cm/s. The firing rates during these high and low motion periods were compared, and a two-sided Wilcoxon rank sum test was used to determine significance between these periods.

Signal to noise ratio (SNR) calculation for *in vivo* photostability evaluation over imaging duration in striatum and hippocampus.

We defined noise as the standard deviation of the fluorescence intensity across the entire trial period. For each neuron, we first calculated the SNR for each action potential by dividing the intensity change observed during an action potential by the noise, and then calculated the average SNRs across all spikes detected in a trial as the corresponding SNR for the trial. For the striatum dataset, only neurons imaged over at least 5 consecutive trials were analyzed. For the hippocampus dataset, all neurons were analyzed.

Detrending.

All optically-recorded SomArchon traces reported in the manuscript (except those in Fig. 4a-d) were corrected for photobleaching or focus shift by subtracting baseline fluorescence traces that were low-pass filtered and fit to a double or single exponential function.

Histology.

Mice were transcardially perfused with PBS followed by 4% paraformaldehyde. The brain was gently extracted from the skull and post-fixed in 4% paraformaldehyde for 1–4 hours at room temperature or overnight at +4°C. Fixed brains were transferred to a 30% sucrose-PBS solution and rotated 24–48 hours at 4C for cryoprotection. Cryoprotected brains were frozen in OCT in a dry ice bath and sliced (coronal) to 50μm thickness using a cryostat. Glial and microglial antibody staining were performed with anti-GFAP[29] (1:250, Clone N206/A8, Neuromab) and anti-Iba1[31] (1:500, 019–19741, Wako Chemicals) primary antibodies, followed by Alexa Fluor 568 (1:1000, Goat anti-Mouse IgG (H+L) Cross-Adsorbed Secondary Antibody, A11004, InVitrogen) and 633 secondary antibodies (1:1000, Goat anti-

Rabbit IgG (H+L) Cross-Adsorbed Secondary Antibody, A21070, InVitrogen). All antibodies were used according to the protocols that have been validated by suppliers. Slice imaging was performed using an inverted Nikon Eclipse Ti microscope equipped with a spinning disk sCSUW1 confocal scanner unit (Yokogawa, Tokyo, Japan), 488, 561, and 642 nm solid state lasers, 525/25 nm, 579/34 nm, and 664LP emission filters, a 20× NA0.75 air objective lens (Nikon), and a 4.2 PLUS Zyla camera (Andor), controlled by NIS-Elements AR software. Acquired images were contrast-enhanced to improve visualization.

Brain temperature measurements.

Under general anesthesia, a craniotomy ~3mm in diameter was made to expose the brain surface, with a small notch on the posterior edge to accommodate the insertion of a temperature probe (Physitemp, IT-1E) coupled to a Thermocouple DAQ (DATAQ Instruments, Model DI-245). An imaging window, identical to those used in all imaging experiments, was positioned on the craniotomy. Kwik sil adhesive was applied around the edges of the imaging window to hold it in place, but not around the craniotomy notch to allow insertion of the temperature probe. Dental cement was then gently applied to affix the imaging window to the skull and to mount an aluminum headbar. Once recovered from anesthesia, mice were head fixed awake and the temperature probe was inserted under the imaging window above the brain surface, through the craniotomy notch. The 637 nm laser was directed through the 40x objective under identical conditions to those used while imaging (75–95mW laser power), and brain temperature was recorded. We noted a temperature increase of 1.88±0.80°C (mean±standard deviation, n = 3 mice) over the 12 second illumination period commonly used in our experiments. These changes are similar to, or smaller than, changes commonly seen with two-photon imaging, optogenetics, and the making of craniotomies for neural imaging[32-36].

Sample size.

No statistical methods were used to estimate sample size for animal studies throughout. We did not perform a power analysis, since our goal was to create a new technology; in the reference (Dell, R. B., Holleran, S. & Ramakrishnan, R. Sample size determination. ILAR. J. 43, 207–213 (2002)), as recommended by the NIH, “In experiments based on the success or failure of a desired goal, the number of animals required is difficult to estimate...” As noted in the aforementioned paper, “The number of animals required is usually estimated by experience instead of by any formal statistical calculation, although the procedures will be terminated [when the goal is achieved].” These numbers reflect our past experience in developing neurotechnologies.

Data exclusions.

Voltage imaging datasets with significant motion or where no spikes were detected were excluded from analysis. Significant motion was defined as a shift for more than 20 μm in any direction. In Extended Data Figure 1i,j,k data points that corresponded to overlapping neurites were excluded. Data exclusion criteria were not pre-established.

Replication.

All attempts at replication were successful.

Randomization and blinding.

There were no treatment conditions to compare in this study. All recording sessions were randomly performed with different voltage sensors or in different brain regions. On recording days, cultured cells or brain slices expressing specific sensors were known. On in vivo recording days, mouse conditions were known. Voltage trace extraction and subsequent analysis were performed with the investigators unaware of specific mouse conditions. For analysis of movement modulation of striatal neuron spiking, a computer algorithm was used to identify periods with different movement parameters. For analysis of spike-phase relationships, or subthreshold membrane voltage relationships, a computer algorithm was used across all conditions. For histology, sections were selected and images were taken from slides by a researcher not aware of the conditions or antibody used. Cells were also counted and quantified from these sections by a researcher blinded to the experimental conditions or antibody used.

Extended Data

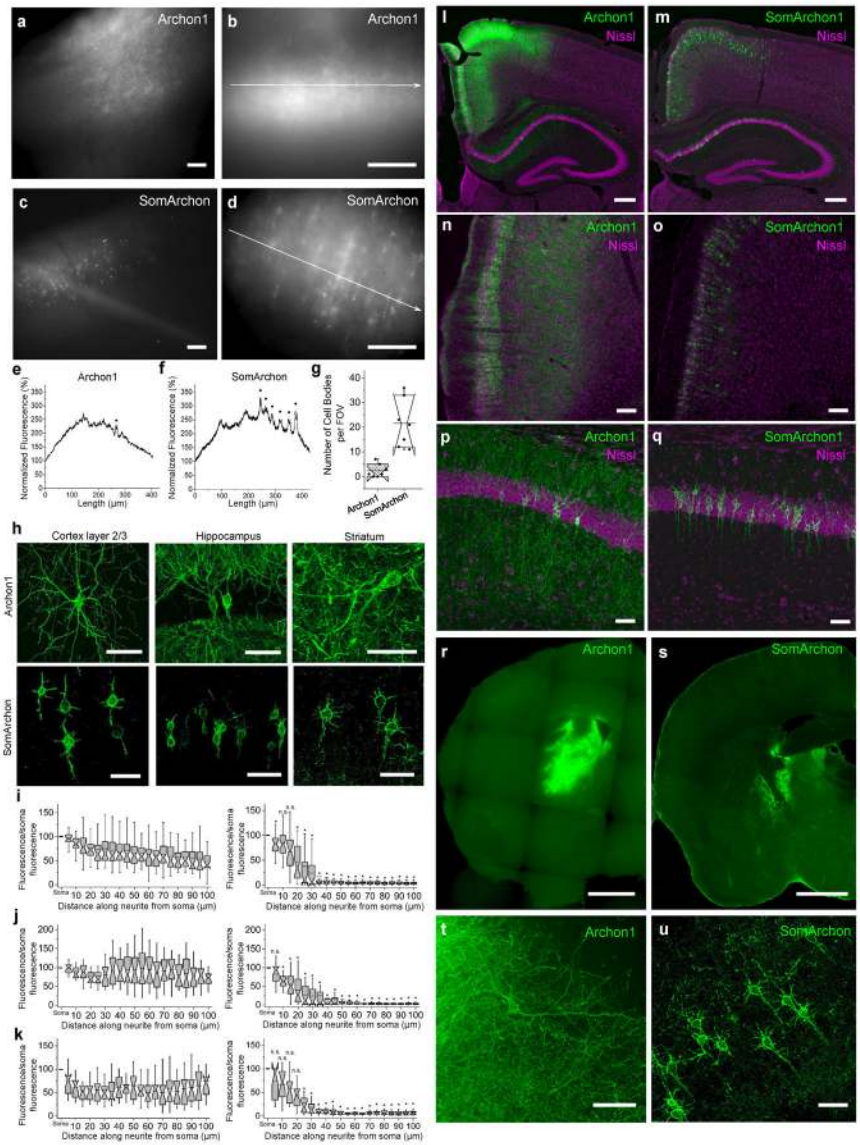

Extended Data Fig. 1. Expression of Archon1 and SomArchon in mouse brain.

(**a**,**b**) Representative Archon1- and (**c**,**d**) SomArchon-expressing mouse brain slices (CAG promoter, via IUE) imaged with a wide-field microscope with (**a**,**c**) 10x and (**b**, **d**) 40x objective lenses (from n = 7 slices from 2 mice each). (**e**, **f**) Normalized EGFP fluorescence along white arrows shown in **b** and **d**. Black dots correspond to resolvable cells. (**g**) Number of resolvable cells per field of view (FOV) for Archon1- and SomArchon-expressing brain slices (2.4 ± 2.5 and 22 ± 9 neurons per FOV (350×415 μm^2) for Archon1 and SomArchon respectively; mean ± standard deviation; n = 7 slices from 2 mice each; boxplots as in Fig. 1). Further confocal analysis with larger FOVs of 500×500×50 μm^3 revealed that SomArchon can resolve ~15 times more neurons in the cortex than Archon1 (n = 4, 8, 9, 11, 11, 18, and 20 neurons from 7 slices for Archon1, versus n=180, 187, and 137 neurons from 3 slices for SomArchon). (**h**) Representative confocal images of neurons in cortex layer 2/3 (left), hippocampus (middle), and striatum (right) expressing Archon1 (top) and SomArchon

(bottom). (**i-k**) EGFP fluorescence along a neurite, normalized to soma, for Archon1- (left) and SomArchon- (right) expressing neurons in (**i**) cortex layer 2/3 (n=39 and 37 neurites from 10 cells from 2 mice each), (**j**) hippocampus (n=20 and 34 neurites from 9 and 17 cells from 2 mice each), and (**k**) striatum (n=17 and 20 neurites from 7 cells from 2 mice each). Box plots as in Fig. 1. n.s.: not significant; *: $p < 0.002$ compared to Archon1 at corresponding position away from the soma; two-sample Kolmogorov-Smirnov test, see Supplementary Table 2. (**l-u**) Representative confocal fluorescence images of Archon (left column) and SomArchon-expressing slices (right column) via (**l-q**) IUE or (**r-u**) AAV injection (green: EGFP; magenta: Nissl staining) in (**n**,**o**) cortex layer 2/3 (n = 8 slices from 2 mice), (**p**,**q**) hippocampus (n = 8 slices from 2 mice), and (**t**,**u**) striatum (n = 6 slices from 2 mice). Scale bars: 100 μm, **a-d**; 50 μm, **h,n-q,t,u**; 250 μm, **l,m,r,s**.

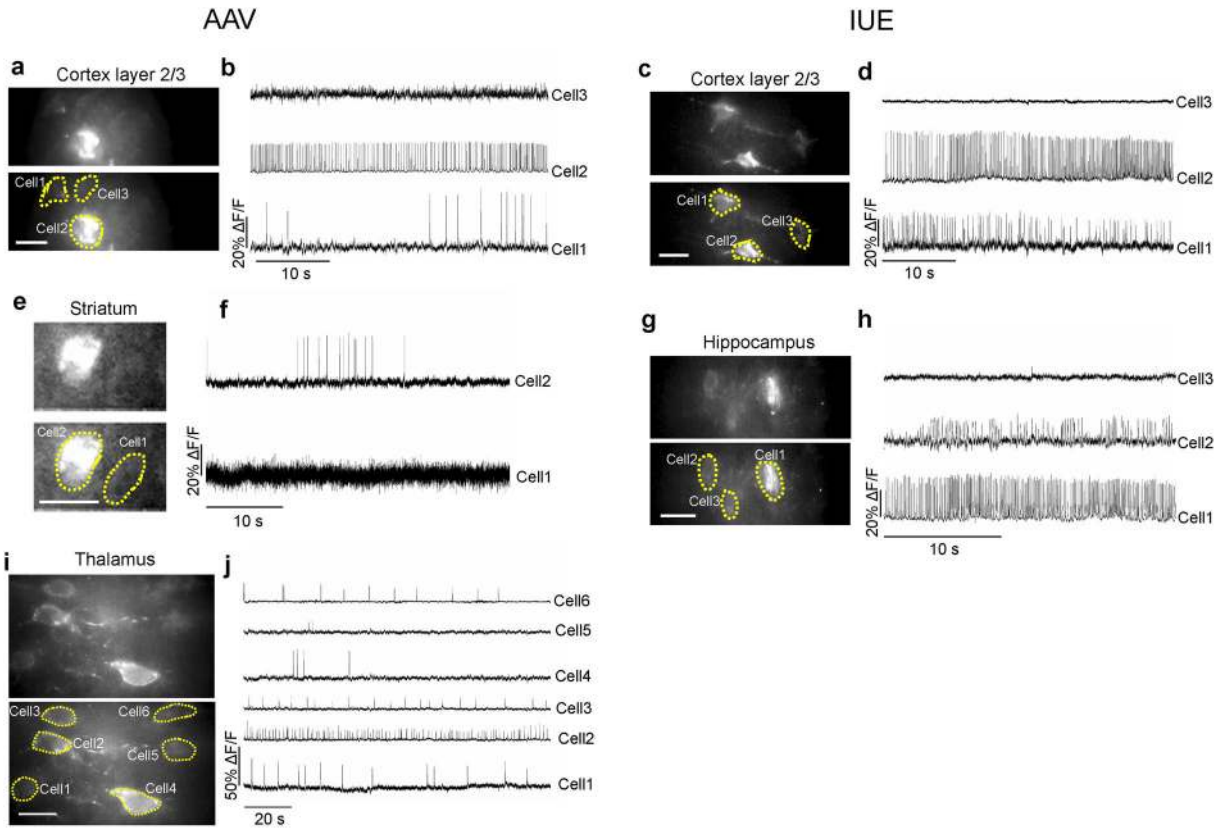

Extended Data Fig. 2. Voltage imaging using SomArchon in mouse brain slices.

(**a-d**) Representative fluorescence wide-field images of cortex layer 2/3 neurons expressing SomArchon via (**a**) AAV transduction or (**c**) IUE with selected ROIs (bottom), and (**b**,**d**) corresponding fluorescence traces (n = 6 and 13 slices from 2 and 4 mice for AAV transduction and IUE, respectively). Acquisition rate: 632 Hz, **b**;, 440Hz, **d**. (**e**) Representative fluorescence wide-field images of striatal neurons expressing SomArchon via AAV transduction (top) with selected ROIs (bottom), and (**f**) corresponding fluorescence traces (n = 8 slices from 2 mice). Acquisition rate: 733 Hz. (**g**) Representative fluorescence wide-field images of hippocampal neurons expressing SomArchon via IUE (top) with selected ROIs (bottom), and (**h**) corresponding fluorescence traces (n = 8 slices from 2 mice). Acquisition rate: 333 Hz. (**i**) Fluorescence wide-field images of thalamus neurons expressing SomArchon (top) via AAV transduction with selected ROIs (bottom), and (**j**) corresponding fluorescence traces (n = 5 slices from 2 mice). Acquisition rate: 333 Hz. Scale bars, 25 μm.

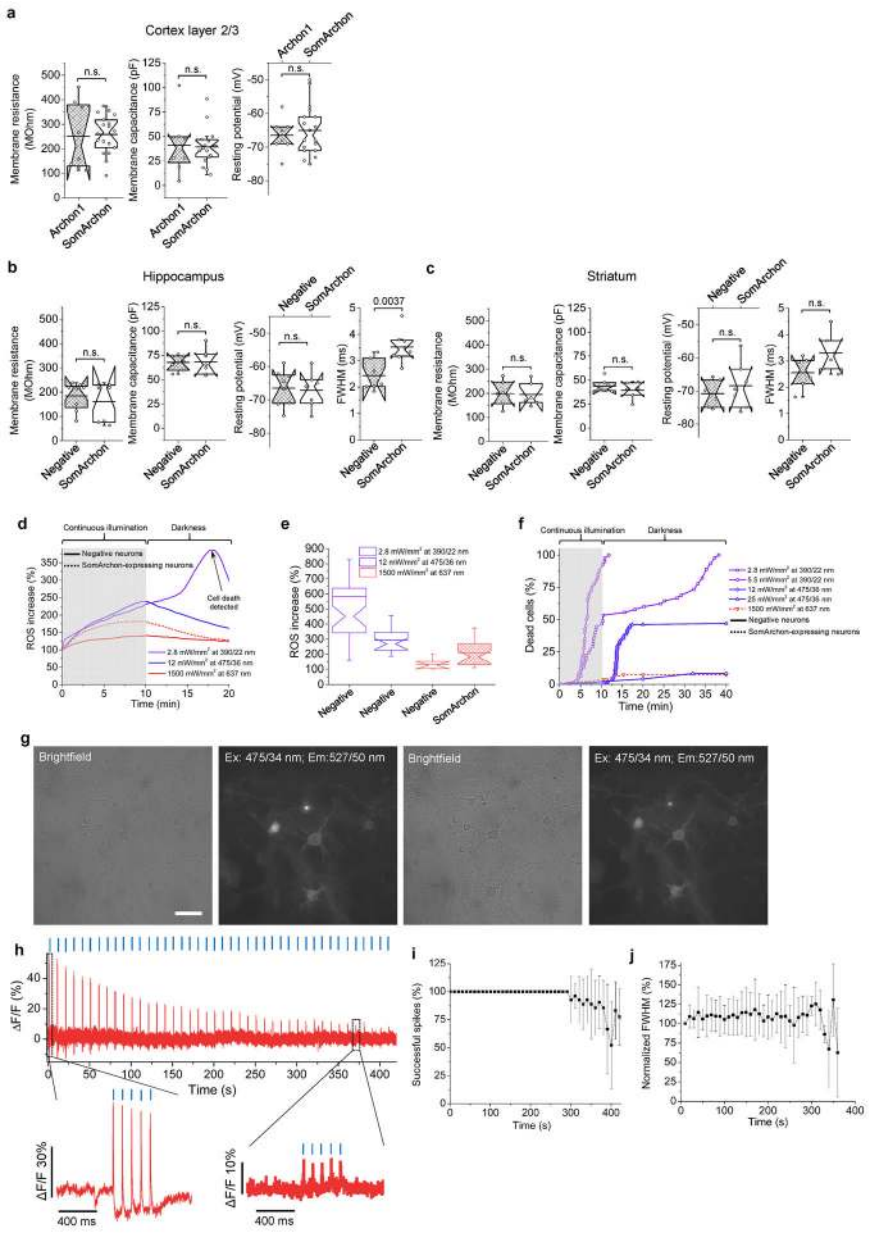

Extended Data Fig. 3. SomArchon expression and voltage imaging do not alter membrane properties or cause phototoxicity.

(**a**) Membrane properties of Archon- (hashed boxes) and SomArchon-expressing (open boxes) neurons in cortex layer 2/3 brain slices (p=0.8026, 0.8895, 0.8236, two-side Wilcoxon Rank Sum test, comparing Archon1 versus SomArchon, for resistance, capacitance, and resting potential respectively; n= 8 and 18 cells from 1 and 2 mice for Archon1 and SomArchon). (**b**) Similar to **a**, but in hippocampus (p=0.6294, 0.9720, 0.8880, 0.0037, two-side Wilcoxon Rank Sum test, comparing negative versus SomArchon for resistance, capacitance, resting potential, FWHM, n = 8 and 7 cells from 2 mice each for negative and SomArchon for resistance and resting potential comparison; n= 7 and 7 cells from 2 mice each for negative and SomArchon for capacitance comparison. FWHM: p=0.0037, n= 7 and 8 cells from from 2 mice each for negative and SomArchon for FWHM

comparison). (**c**) Similar to **a**, but in striatum (p=0.7380, 0.8357, 0.7751, 0.0931, two-side Wilcoxon Rank Sum test, comparing negative and SomArchon, for resistance, capacitance, resting potential and FWHM; n = 7 and 6 cells from 2 mice each for negative and SomArchon for resistance and capacitance comparisons; n = 6 and 7 cells from 2 mice each for negative and SomArchon for resting potential comparison; n = 6 and 6 cells from 2 mice each for negative and SomArchon for FWHM comparisons). (**d**) Changes of relative reactive oxygen species (ROS) concentration (normalized to that before illumination) over time in negative (solid line) and SomArchon-expressing (dashed line) cultured mouse neurons under various illumination protocols. (**e**) Maximal increase in ROS concentration during continuous illumination for conditions performed in **d** (n=45, 24, and 8 negative neurons from 2, 2, and 1 cultures for 390/22 nm, 475/36 nm, and 637 nm illumination, respectively; n = 24 SomArchon-expressing neurons for 637 nm illumination from 1 culture). (**f**) Cell death for negative (solid line) and SomArchon-expressing (dashed line) cultured neurons at DIV 14–18 under various illumination protocols. (n=45, 35, 91, 40, and 27 neurons from 2, 1, 2, 1, and 1 cultures respectively for 390/22 nm at 2.8 mW/mm^2, 390/22 nm at 5.5 mW/mm^2, 475/36 nm at 12 mW/mm^2, 475/36 nm at 25 mW/mm^2, and 637 nm at 1500 mW/mm^2 illumination). (**g**) Bright-field and fluorescence images of representative neurons expressing SomArchon before and after 10 min of continuous 637nm laser illumination at 1500 mW/mm^2, followed by 10 min in darkness (93% of imaged cells did not exhibit noticeable changes in morphology; n = 27 cells from 1 culture; non-illuminated cells did not show any changes in morphology; n = 10 cells from 1 cultures). Scale bar, 50 μm. (**h**) Representative SomArchon fluorescence trace from neuron co-expressing SomArchon and CoChR-$K_v2.1_{motif}$. (**i**) Normalized spike rates (to initial value) elicited by blue light illumination dropped after 300 s of continuous recording, due to decrease in spike amplitude as a result of photobleaching (n = 10 neurons from 1 culture; plotted as mean ± standard deviation). (**j**) Normalized (to initial value) full width half maximum (FWHM) of spikes elicited by continuous light exposure as in **h**. Box plots displayed as in Fig. 1.

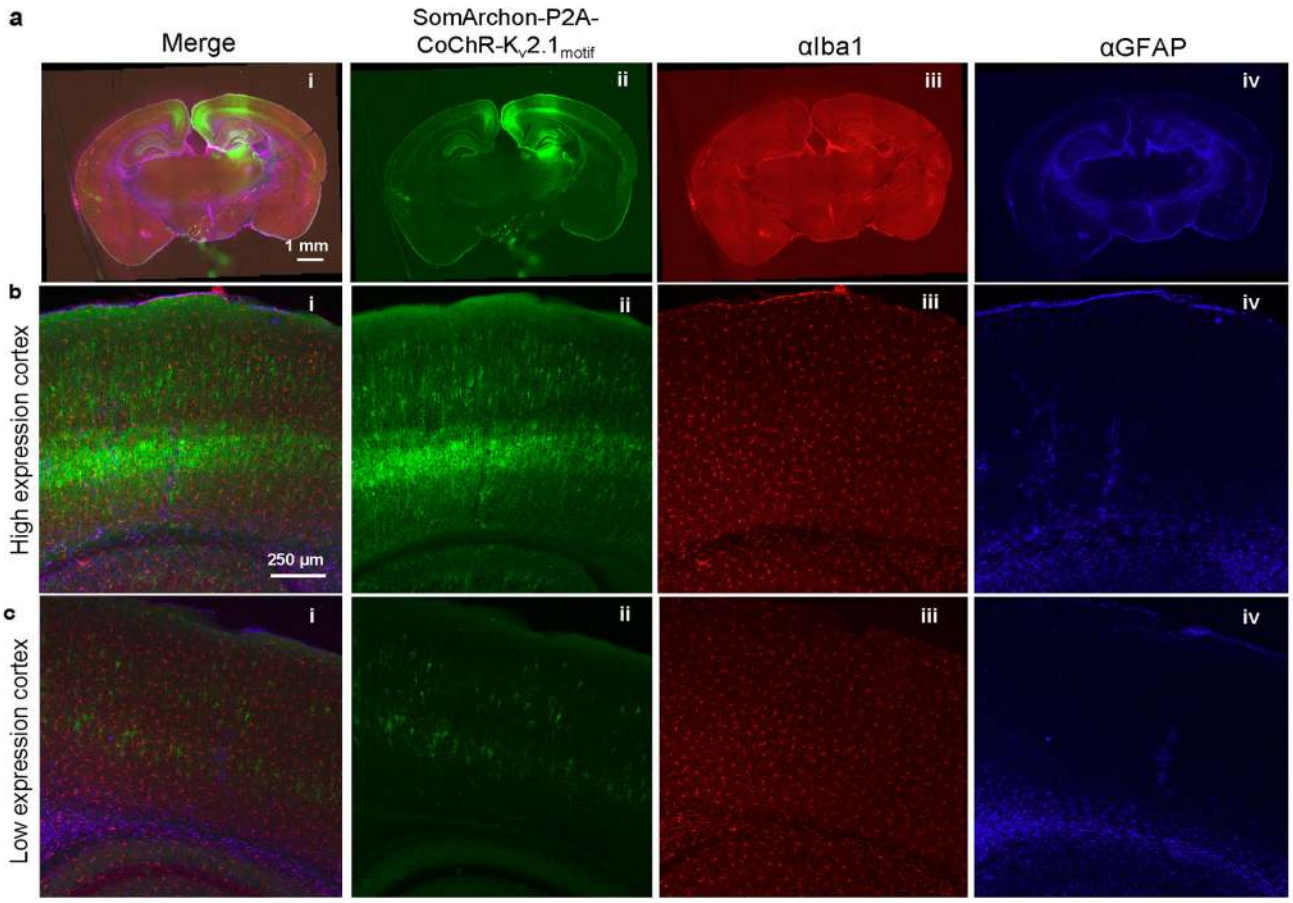

Extended Data Fig. 4. SomArchon expression *in vivo* does not cause gliosis.

SomArchon was expressed in the mouse brain by AAV2.9-Syn-SomArchon-P2A-CoChR-$K_V2.1_{motif}$ injection into the cortex in P0 Swiss Webster mice. Brain tissues were analyzed 63 days post viral injection. (i) Merged fluorescence images from 50 μm-thick coronal sections were visualized via (ii) EGFP fluorescence of SomArchon, (iii) anti-Iba1 immunofluorescence, and (iv) anti-GFAP immunofluorescence (n = 4 slices from 2 mice). (**a**) Expression throughout the coronal section. (**b**) Zoomed-in view on the virally injected area (high expression cortex). (**c**) Zoomed-in view on the non-injected contralateral hemisphere (low expression cortex). GFAP and Iba1, commonly used glial and microglial markers, showed similar appearance on the virally injected hemisphere versus the non-injected hemisphere, suggesting that expression of SomArchon did not cause gliosis. Scale bars: 1 mm, **a**; and 250 μm, **b**,**c**.

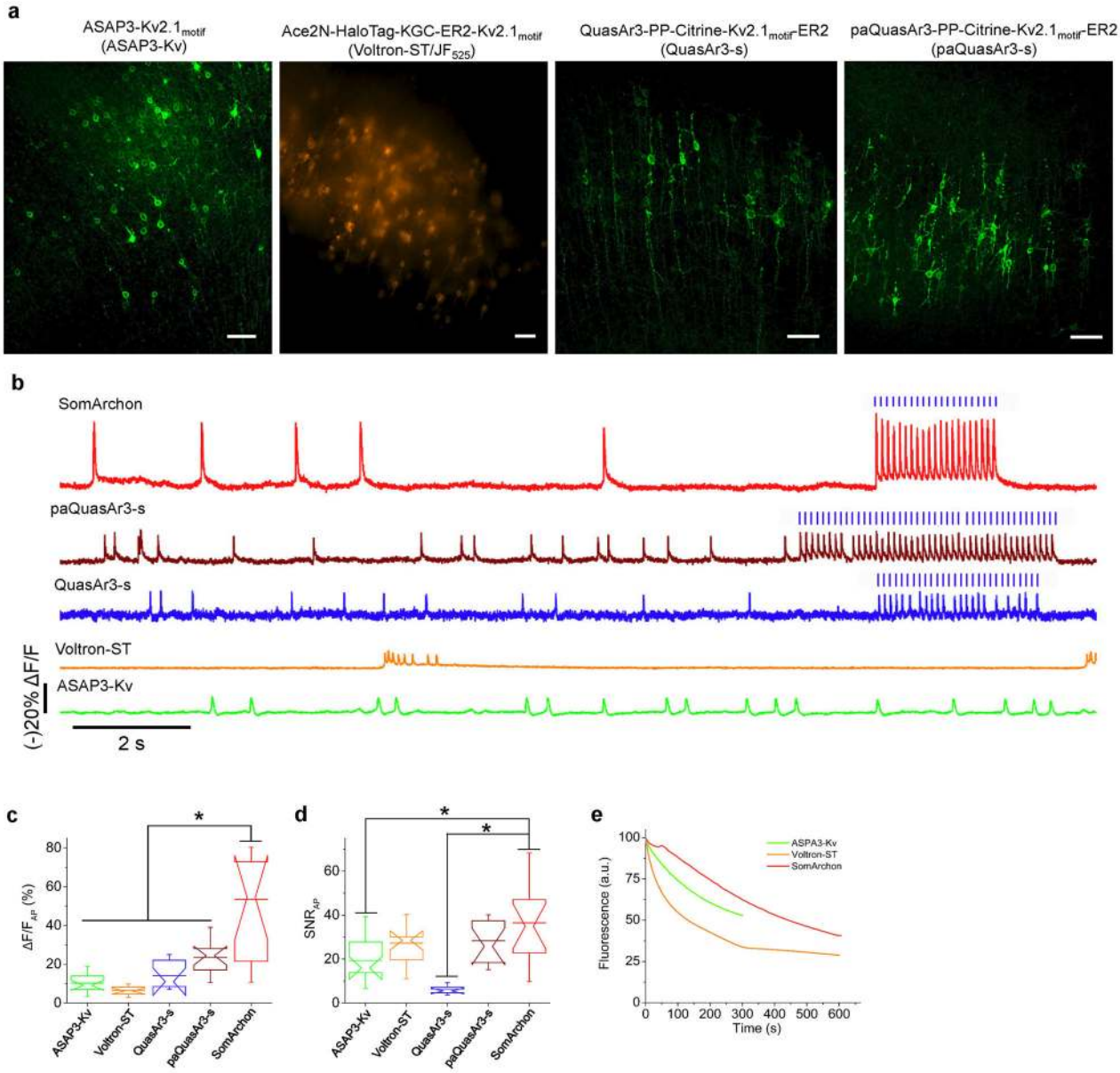

Extended Data Fig. 5. Side-by-side comparison of next-generation voltage indicators in mouse brain slices.

(**a**) Representative fluorescence images of mouse cortex layer 2/3 neurons expressing ASAP3-$K_V2.1_{motif}$ (ASAP3-Kv), Ace2N-HaloTag-KGC-ER2-$K_V2.1_{motif}$ (Voltron-ST), QuasAr3-PP-mCitrine-$K_V2.1_{motif}$-ER2 (QuasAr3-s), and paQuasAr3-PP-mCitrine-$K_V2.1_{motif}$-ER2 (paQuasAr3-s). ASAP3-Kv, QuasAr3-s and paQuasAr3-s were visualized via cpGFP, mCitrine, and mCitrine fluorescence respectively, using laser excitation at 488 nm and emission at 525/50 nm under a confocal microscope. Voltron-ST was visualized via JF525 fluorescence using LED excitation at 510/25 nm and emission at 545/40 nm under a wide-field microscope. Scale bar, 50 μm. (**b**) Single-trial optical recordings of ASAP3-Kv (green) and Voltron-ST/JF525 (orange) fluorescence responses during 4-aminopyridine evoked neuronal activity, and QuasAr3-s (blue), paQuasAr3-s (brown), and SomArchon

(red) fluorescence responses during CoChR-mTagBFP2-$K_V2.2_{motif}$ evoked neuronal activity. Acquisition rate ~500 Hz. Blue light pulses (470/20nm, 2ms per pulse, 10Hz), shown as vertical blue bars, were used to activate CoChR to evoke spiking. (**c,d**) Quantification of (**c**) ΔF/F and (**d**) signal-to-noise ratio (SNR) per AP across all recordings (n=18, 14, 9, 13, and 14 neurons from 1, 2, 2, 2, and 2 mice for ASAP3-Kv, Voltron-ST/JF525, QuasAr3-s, paQuasAr3-s, and SomArchon, respectively). Box plots displayed as in Fig. 1. (*$p < 0.01$, Wilcoxon rank sum test; see Supplementary Table 2 for statistics) (**e**) Photobleaching curves of ASAP3-Kv, Voltron-ST/JF525, and SomArchon under continuous illumination (n=11, 8, and 17 neurons from 1 culture, respectively).

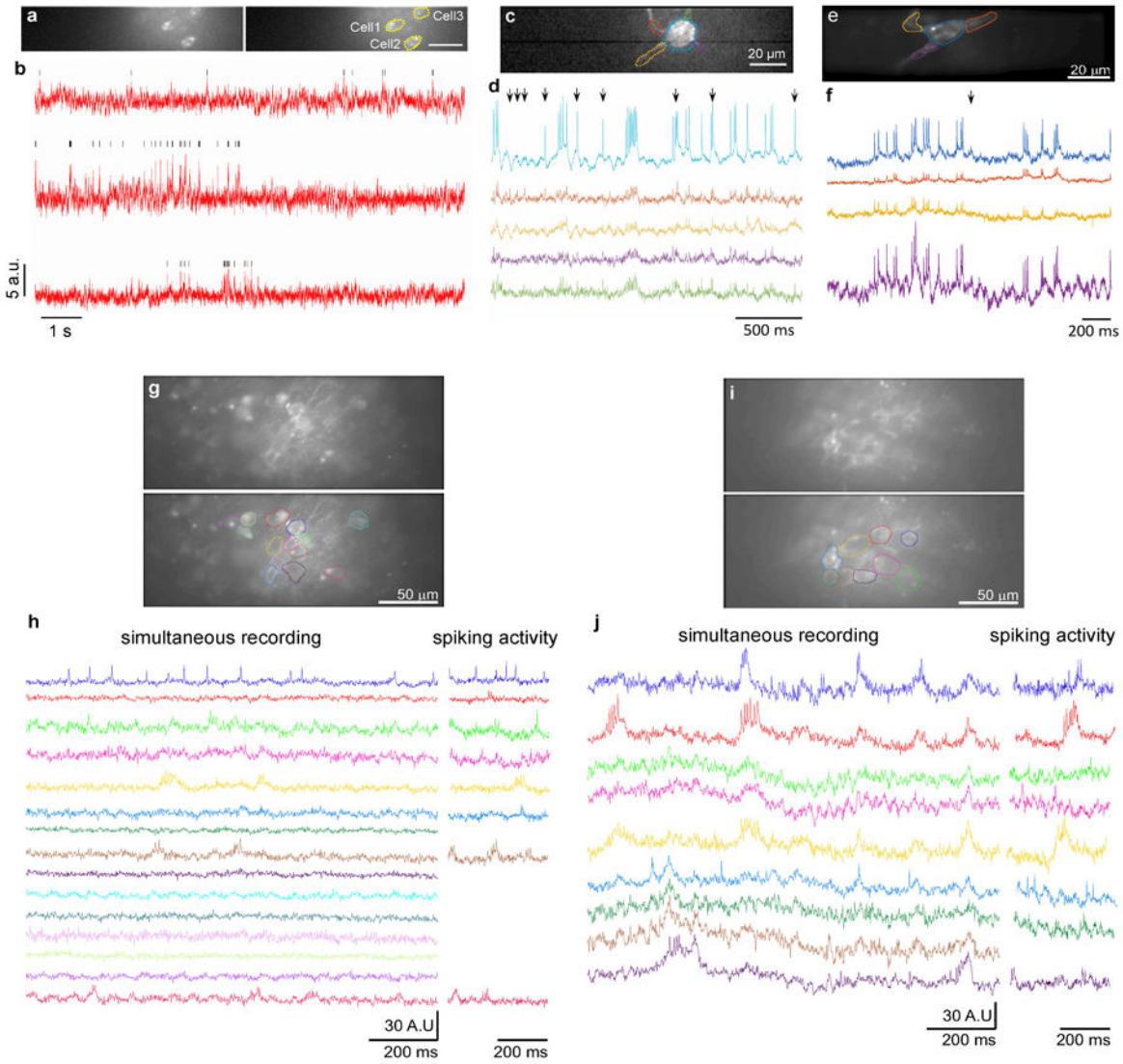

Extended Data Fig. 6. SomArchon enables both local dendritic and population imaging of neurons in multiple brain regions *in vivo*.

(**a**) Fluorescence images of selected FOV in motor cortex (left) with selected ROIs corresponding to somas of three neurons (right) (n = 1 FOV from 1 mouse). Scale bar, 50 μm. (**b**) Representative fluorescence traces from **a** with detected spikes (black ticks). (**c**) Fluorescence image of a hippocampal neuron expressing SomArchon with ROIs selected at the soma and on four proximal dendrites (n = 1 neuron from 1 mouse). Scale bar, 20 μm. (**d**) Optical voltage traces from the selected ROIs shown in **c**. (**e**) Fluorescence image of a striatal neuron expressing SomArchon with ROIs selected at the soma and on three proximal dendrites (n = 1 neuron from 1 mouse). Scale bar, 20 μm. (**f**) Optical voltage traces from the selected ROIs shown in **e**. Black arrows highlight example instances when dendritic voltages visibly differed from those on the soma. (**g-k**) *In vivo* population voltage imaging in the hippocampus CA1 region (n = 14 FOVs from 3 mice). (**g**, **i**) Average intensity projection image for each video (top), and with identified ROIs (bottom). (**h**, **j**) Optical voltage traces for each neuron shown in **g,i**, respectively, with colors matching corresponding ROI colors.

Shown are 1.2 seconds of simultaneously recorded voltage for all neurons (left), and a zoomed-in period with prominent spikes (right). Image acquisition rate for all recordings: 826 Hz.

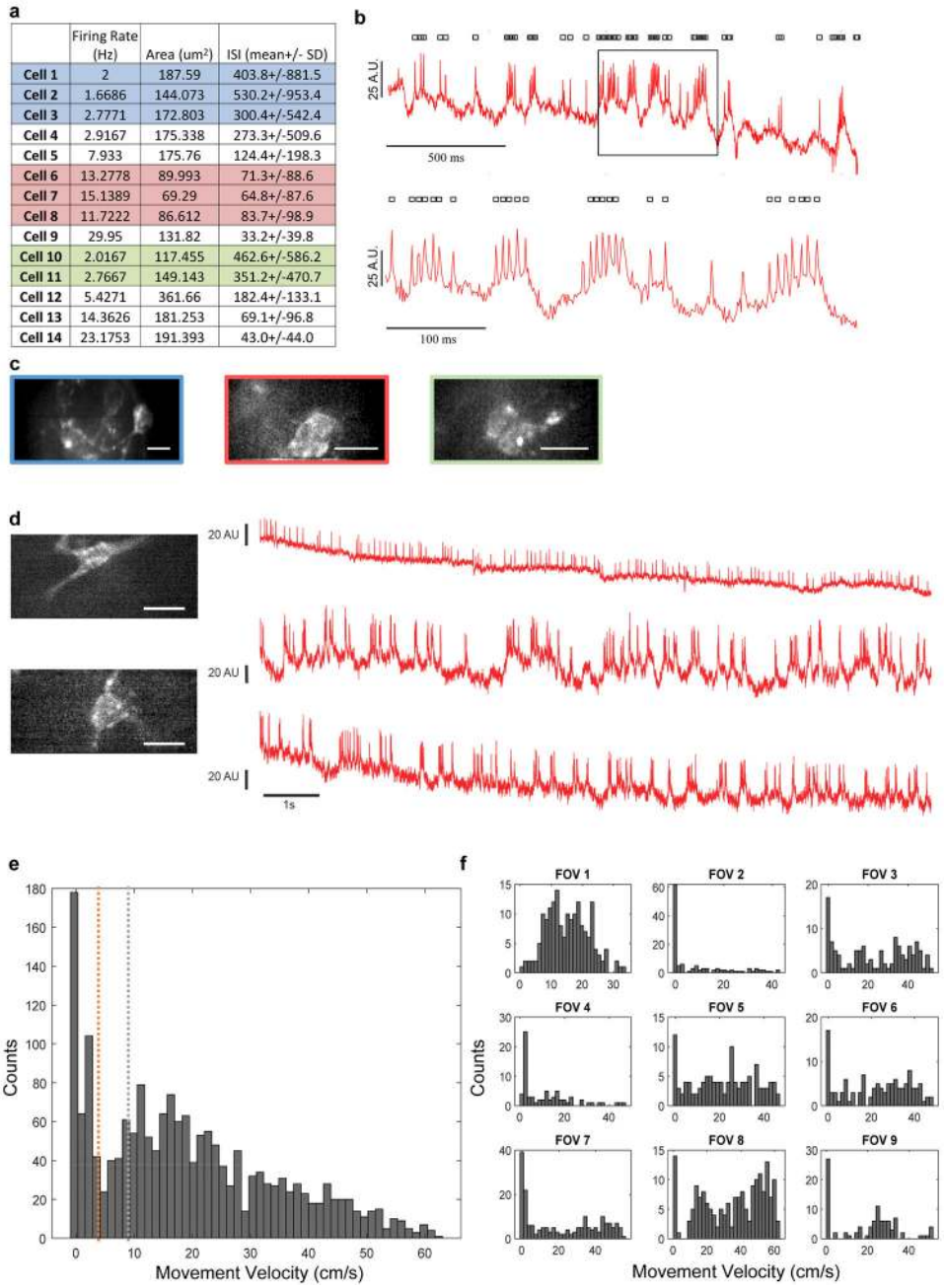

	Firing Rate (Hz)	Area (um²)	ISI (mean+/- SD)
Cell 1	2	187.59	403.8+/-881.5
Cell 2	1.6686	144.073	530.2+/-953.4
Cell 3	2.7771	172.803	300.4+/-542.4
Cell 4	2.9167	175.338	273.3+/-509.6
Cell 5	7.933	175.76	124.4+/-198.3
Cell 6	13.2778	89.993	71.3+/-88.6
Cell 7	15.1389	69.29	64.8+/-87.6
Cell 8	11.7222	86.612	83.7+/-98.9
Cell 9	29.95	131.82	33.2+/-39.8
Cell 10	2.0167	117.455	462.6+/-586.2
Cell 11	2.7667	149.143	351.2+/-470.7
Cell 12	5.4271	361.66	182.4+/-133.1
Cell 13	14.3626	181.253	69.1+/-96.8
Cell 14	23.1753	191.393	43.0+/-44.0

Extended Data Fig. 7. Properties of striatal neurons and movement thresholds.

(**a**) Average firing rate, size, and interspike interval (ISI) for the 14 neurons recorded in 9 FOV in 2 mice. Cells simultaneously recorded in the same FOV are color-coded (blue, red, green). Cells in rows with a white background were recorded individually. (**b**) Selected trace from Cell 9 exhibiting spike bursting (top), and a zoomed view of the boxed region (bottom). A.U. arbitrary unit. Identified spikes are indicated by the black dots on top of the trace. (**c**) Single frame images for FOVs with multiple neurons. Each FOV is color-coded to match **a**. Scale bars, 20 μm. (**d**) Representative optical traces of two striatal cholinergic interneurons from Cre-dependent SomArchon-expressing in a ChAT-Cre mouse (left, scale

bar, 20 μm), recorded in 3 sessions, while mouse was awake, head-fixed and navigating a spherical treadmill (n = 2 neurons from 1 mouse). Two bottom traces are from the same neuron, left, bottom. Image acquisition rate, 826 Hz. (**e**) Histogram of instantaneous movement speeds for all FOVs shown in Fig. 3 (9 FOVs in 2 mice). Instantaneous movement speed was calculated as average speed during each 0.5-second time interval. Red line, threshold for low movement speed identification; green line, threshold for high movement speed identification. (**f**) Histogram of instantaneous movement speed for individual FOVs analyzed.

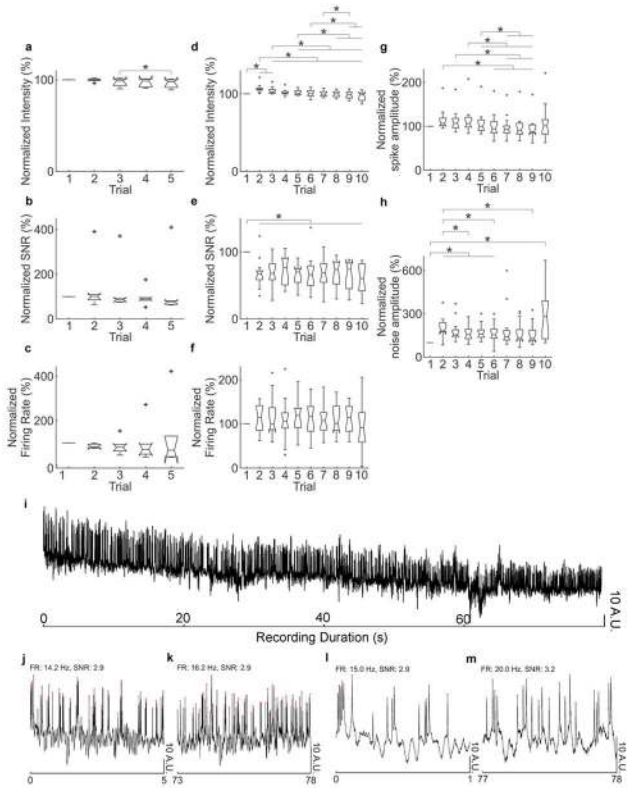

Extended Data Fig. 8. *In vivo* SomArchon performance over time in the striatum and hippocampus of awake mice.

(**a-h**) Average fluorescence intensity, SNR per spike, and firing rates of neurons in the striatum and hippocampus of awake mice, over multiple trials. (**a-c**) In each striatal recording session, we performed 5 trials, each 12 seconds long, with inter-trial intervals of 30–60 seconds. (**a**) Average fluorescence intensity decreased slightly, while (**b**) spike SNR and (**c**) firing rates remained constant throughout the recording session (repeated measures ANOVA, n = 6 neurons in 5 FOVs from one mouse). (**d-h**) In each hippocampal recording session, we performed 10 trials, each 6 seconds long, with inter-trial intervals of 20–30 seconds. (**d**) Average fluorescence intensity showed a slight but significant decrease across trials. (**e**) SNR decreased between the 1st and 2nd trials but not afterwards, and (**f**) the firing rate remained constant. (**g**) Spike amplitude fluctuated randomly over trials, and (**h**) there was a significant increase in baseline noise between the 1st and 2nd trials (repeated measures ANOVA; *: p<0.05, post-hoc test: Tukey's HSD test, n = 16 neurons in 7 FOVs from 4 mice, see Supplementary Table 2). Measurements were normalized to the first trial for each neuron. All box plots displayed are as in Fig. 4. (**i-m**) A representative continuous optical trace of a hippocampal neuron over 80 seconds in an awake, head-fixed mouse, with zoomed-in view (**j-m**) at the beginning and end of the recording highlighting comparable firing rates and SNRs (n = 16 neurons in 7 FOVs from 4 mice).

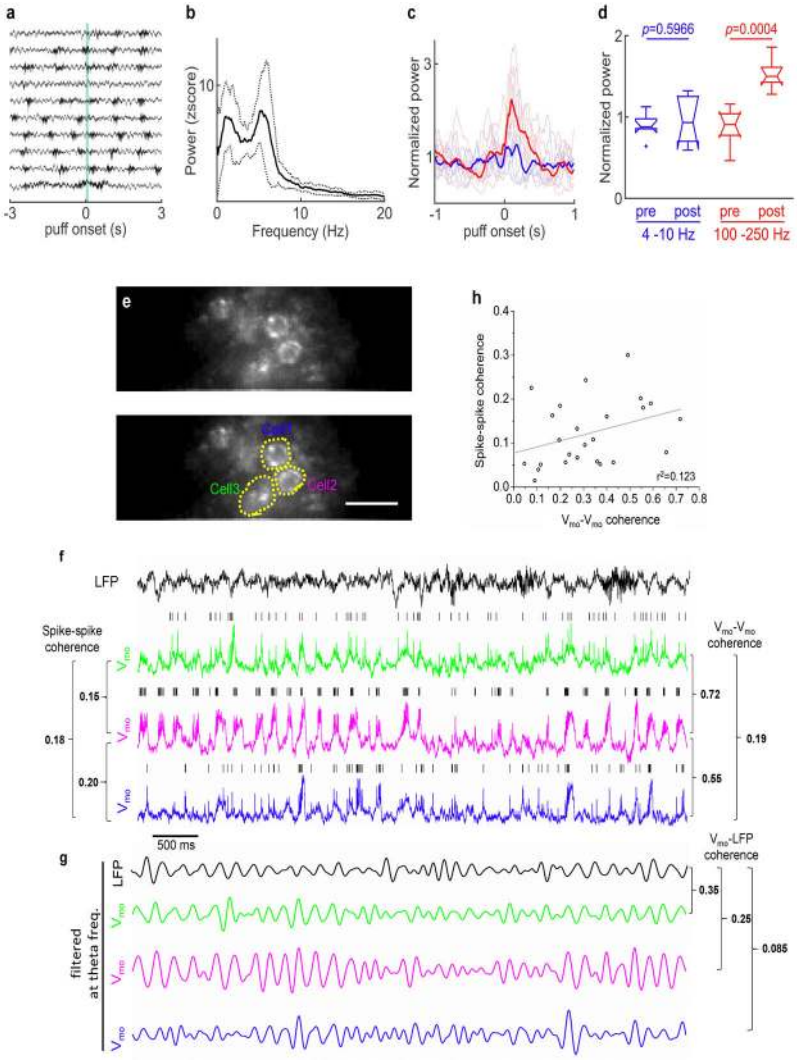

Extended Data Fig. 9. LFP and subthreshold membrane voltage oscillation analysis in the hippocampus.

(**a**) Example hippocampal LFP recordings from a session with 10 trials, aligned to the onset of an air puff (green shading) directed to one eye in awake headfixed mice. (**b**) LFP power spectrum shows strong theta oscillations. Plotted are mean±standard deviation, n=10 trials in 1 session. (**c**) Oscillation power at high frequencies (100–250 Hz, red) and at theta frequencies (blue), aligned to puff onset. Each thin line represents an individual recording session, and the thick lines denote means (n = 7 sessions in 4 mice). (**d**) Eye puff evoked a significant increase in LFP power at high frequency, but not at theta frequency (theta frequency: $p = 0.5966$, high frequency: $p = 0.0004$, two-tailed paired Student's t-test, n=7 sessions in 4 mice). Box plots are as in Fig. 4. (**e**) Fluorescence image of a representative FOV (top) with selected ROIs (bottom). (**f**) Membrane voltage recorded optically (V_{mo}) from neurons identified in **e**, and simultaneously recorded LFPs. Black vertical ticks above V_{mos} denote spikes. Spike-spike coherence values between neurons are shown at the left and V_{mo}-V_{mo} theta coherence values are shown at the right. (**g**) Theta frequency-filtered LFPs and V_{mos} for the four traces shown in **f**. V_{mo}-LFP coherence values are shown to the right.

(**h**) Scatter plot of V_{mo}-V_{mo} theta frequency coherence and spike-spike coherence from all neuron pairs, fitted with a linear regression (n=25 pairs, p=0.08, t-statistic, r^2=0.12).

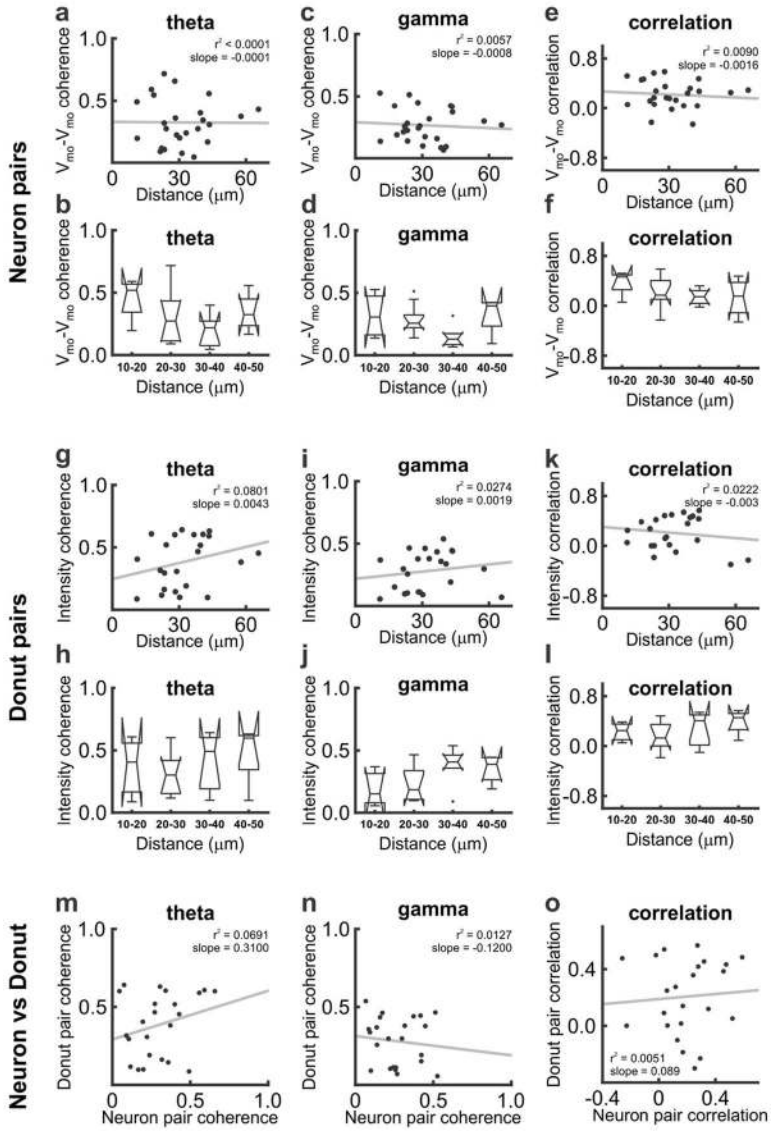

Extended Data Fig. 10. Pair-wise coherence and correlation measures over spatial distance.

To investigate the potential of background fluorescence signals under wide-field imaging to produce shared crosstalk signals on neuron pairs, we examined the relationship of various coherence and correlation measures between neurons and background fluorescence over spatial distance. (**a-b**) Pair-wise coherence at theta frequencies between neurons. V_{mo}-V_{mo} coherence did not decrease significantly with spatial distance. (**a**, n=25 pairs analyzed with spatial distance of 11–66 μm, center to center; **b**, n=23 pairs within 50 μm of each other, F=1.44, p=0.26, one-way ANOVA). (**c, d**) Pair-wise V_{mo}-V_{mo} coherence at gamma frequencies (30–50 Hz) was not dependent on spatial distance (**c**, n=25 pairs); **d**, n=23 pairs within 50 μm of each other, F=2.10, p=0.13, one-way ANOVA). **(e**, **f)** Pair-wise correlation between neurons did not decrease significantly with spatial distance (**e**, n=25 pairs; **f**, n=23 pairs within 50 μm, F=1.00, p=0.42, one-way ANOVA). (**g-l**) Same analysis as in **a-f** performed in background donut ROIs surrounding each neuron (for donut definition see Methods). Similar to results from neuron pairs, we found that theta frequency coherence

between background donut ROIs was not dependent on spatial distance (**g**, n=23 pairs; **h**, n=21 pairs, F=0.65, p=0.59, one-way ANOVA), nor was gamma frequency coherence (**I**, n=23 pairs; **j**, n=21 pairs, F=1.93, p=0.16, one-way ANOVA), nor was the correlation coefficient (**k**, n=23 pairs; **l**, n=21 pairs, F=1.02, p=0.41, one-way ANOVA). (**m-o**) The coherence between neurons and their corresponding donuts were not correlated, at theta frequency (**m**) or at gamma frequency (**n**), or for the Pearson correlation coefficients (**o**). All box plots displayed are as in Fig. 4.

Supplementary Material

Refer to Web version on PubMed Central for supplementary material.

Acknowledgments

We thank Tina Ta for her help on histology. We thank M. Murdock for help with animal work, N. Pak and A. Badon and J. Mertz for help with assembling the *in vivo* imaging setup. We also thank Yosuke Bando for helping with the supplemental video.

Funding

E.S.B. acknowledges funding from Edward and Kay Poitras, NIH Director's Pioneer Award 1DP1NS087724, NIH 1R01GM104948, NIH 1R01EB024261, NIH 1R01DA045549, NIH 1R01MH114031, Charles Hieken, NIH 1R01NS102727, John Doerr, NSF Grant 1734870, the HHMI-Simons Faculty Scholars Program, Human Frontier Science Program RGP0015/2016, NIH 1R43MH109332, U. S. Army Research Laboratory and the U. S. Army Research Office under contract/grant number W911NF1510548, NIH 2R01DA029639, and NSF CBET 1344219. X.H. acknowledges funding from NIH Director's Office (1DP2NS082126), NINDS (1R01NS081716, 1R01NS087950–01), the Grainger Foundation, the Pew Foundation, Boston University Biomedical Engineering Department. S.B. and S.N.S. acknowledge funding from the NIH/NIGMS T32 Quantitative Biology and Physiology Fellowship (GM008764) through the Boston University Biomedical Engineering department. The funders had no role in study design, data collection and analysis, decision to publish, or preparation of the manuscript.

References

1. Hochbaum DR et al. All-optical electrophysiology in mammalian neurons using engineered microbial rhodopsins. Nat. Methods 11, 825–33 (2014). [PubMed: 24952910]
2. St-Pierre F et al. High-fidelity optical reporting of neuronal electrical activity with an ultrafast fluorescent voltage sensor. Nat. Neurosci. 17, 884–9 (2014). [PubMed: 24755780]
3. Gong Y, Wagner MJ, Li JZ & Schnitzer MJ Imaging neural spiking in brain tissue using FRET-opsin protein voltage sensors. Nat. Commun. 5, 1–11 (2014).
4. Adam Y et al. Voltage imaging and optogenetics reveal behaviour-dependent changes in hippocampal dynamics. Nature 569, 413–417 (2019). [PubMed: 31043747]
5. Chavarha M et al. Fast two-photon volumetric imaging of an improved voltage indicator reveals electrical activity in deeply located neurons in the awake brain. bioRxiv (2018).
6. Abdelfattah AS et al. Bright and photostable chemigenetic indicators for extended in vivo voltage imaging. bioRxiv (2018).
7. Gong Y et al. High-speed recording of neural spikes in awake mice and flies with a fluorescent voltage sensor. Sciencexpress 350, 1–11 (2015).
8. Lou S et al. Genetically Targeted All-Optical Electrophysiology with a Transgenic Cre-Dependent Optopatch Mouse. J. Neurosci. 36, 11059–11073 (2016). [PubMed: 27798186]
9. Jin X, Tecuapetla F & Costa RM Basal ganglia subcircuits distinctively encode the parsing and concatenation of action sequences. Nat. Neurosci. 17, 423–430 (2014). [PubMed: 24464039]
10. Shi LH, Luo F, Woodward DJ & Chang JY Neural responses in multiple basal ganglia regions during spontaneous and treadmill locomotion tasks in rats. Exp. Brain Res. 157, 303–314 (2004). [PubMed: 15067433]

11. Gritton HJ et al. Unique contributions of parvalbumin and cholinergic interneurons in organizing striatal networks during movement. Nat. Neurosci. 22, 586–597 (2019). [PubMed: 30804530]
12. Flytzanis NC et al. Archaerhodopsin variants with enhanced voltage-sensitive fluorescence in mammalian and Caenorhabditis elegans neurons. Nat. Commun. 5, 4894 (2014). [PubMed: 25222271]
13. Piatkevich KD et al. A robotic multidimensional directed evolution approach applied to fluorescent voltage reporters. Nature Chemical Biology 14, 901 (2018).
14. Jin L et al. Single Action Potentials and Subthreshold Electrical Events Imaged in Neurons with a Fluorescent Protein Voltage Probe. Neuron 75, 779–785 (2012). [PubMed: 22958819]
15. Chamberland S et al. Fast two-photon imaging of subcellular voltage dynamics in neuronal tissue with genetically encoded indicators. Elife 6, 1–35 (2017).
16. Zou P et al. Bright and fast multicoloured voltage reporters via electrochromic FRET. Nat. Commun 5, 4625 (2014). [PubMed: 25118186]
17. Gong Y et al. High-speed recording of neural spikes in awake mice and flies with a fluorescent voltage sensor. Science (80-.). 350, 1–11 (2015).
18. Shemesh OA et al. Temporally precise single-cell-resolution optogenetics. Nat. Neurosci. 20, (2017).
19. Baker CA, Elyada YM, Parra A & Bolton MML Cellular resolution circuit mapping with temporal-focused excitation of soma-targeted channelrhodopsin. Elife 5, 1–15 (2016).
20. Daigle TL et al. A Suite of Transgenic Driver and Reporter Mouse Lines with Enhanced Brain-Cell-Type Targeting and Functionality. Cell (2018). doi:10.1016/j.cell.2018.06.035
21. Wu C, Ivanova E, Zhang Y & Pan ZH rAAV-Mediated Subcellular Targeting of Optogenetic Tools in Retinal Ganglion Cells In Vivo. PLoS One 8, 1–10 (2013).
22. Klapoetke NC et al. Independent optical excitation of distinct neural populations. Nat. Methods 11, 338–46 (2014). [PubMed: 24509633]
23. Kravitz AV & Kreitzer AC Striatal Mechanisms Underlying Movement, Reinforcement, and Punishment. Physiology 27, 167–177 (2012). [PubMed: 22689792]
24. Koós T & Tepper JM Inhibitory control of neostriatal projection neurons by GABAergic interneurons. Nat. Neurosci. 2, 467–472 (1999). [PubMed: 10321252]
25. Zhou FM, Wilson CJ & Dani JA Cholinergic interneuron characteristics and nicotinic properties in the striatum. J. Neurobiol. 53, 590–605 (2002). [PubMed: 12436423]
26. Bittner KC et al. Conjunctive input processing drives feature selectivity in hippocampal CA1 neurons. Nat. Neurosci. 18, 1133–1142 (2015). [PubMed: 26167906]
27. Harvey CD, Collman F, Dombeck DA & Tank DW Intracellular dynamics of hippocampal place cells during virtual navigation. Nature 461, 941–946 (2009). [PubMed: 19829374]

References for Methods

28. Adam Y et al. All-optical electrophysiology reveals brain-state dependent changes in hippocampal subthreshold dynamics and excitability. bioRxiv (2018). doi:10.1101/281618
29. Hansen KR, Dewalt GJ, Mohammed AI, Tseng H & Moona E Mild Blast Injury Produces Acute Changes in Basal Intracellular Calcium Levels and Activity Patterns in Mouse Hippocampal. 1–42 (2017). doi:10.1089/neu.2017.5029
30. Dombeck DA, Khabbaz AN, Collman F, Adelman TL & Tank DW Imaging Large-Scale Neural Activity with Cellular Resolution in Awake, Mobile Mice. Neuron 56, 43–57 (2007). [PubMed: 17920014]
31. Fields IE et al. Noninvasive Deep Brain Stimulation via Temporally Article Noninvasive Deep Brain Stimulation via Temporally Interfering Electric Fields. Cell 169, 1029–1041.e16
32. Kalmbach AS & Waters J Brain surface temperature under a craniotomy. J. Neurophysiol. (2012). doi:10.1152/jn.00557.2012
33. Podgorski K & Ranganathan G Brain heating induced by near-infrared lasers during multiphoton microscopy. J. Neurophysiol. 116, 1012–1023 (2016). [PubMed: 27281749]

34. Arias-Gil G, Ohl FW, Takagaki K & Lippert MT Measurement, modeling, and prediction of temperature rise due to optogenetic brain stimulation. Neurophotonics (2016). doi:10.1117/1.nph.3.4.045007

35. Stujenske JM, Spellman T & Gordon JA Modeling the Spatiotemporal Dynamics of Light and Heat Propagation for InVivo Optogenetics. Cell Rep. 12, 525–534 (2015). [PubMed: 26166563]

36. Christie IN et al. FMRI response to blue light delivery in the naïve brain: Implications for combined optogenetic fMRI studies. Neuroimage (2013). doi:10.1016/j.neuroimage.2012.10.074

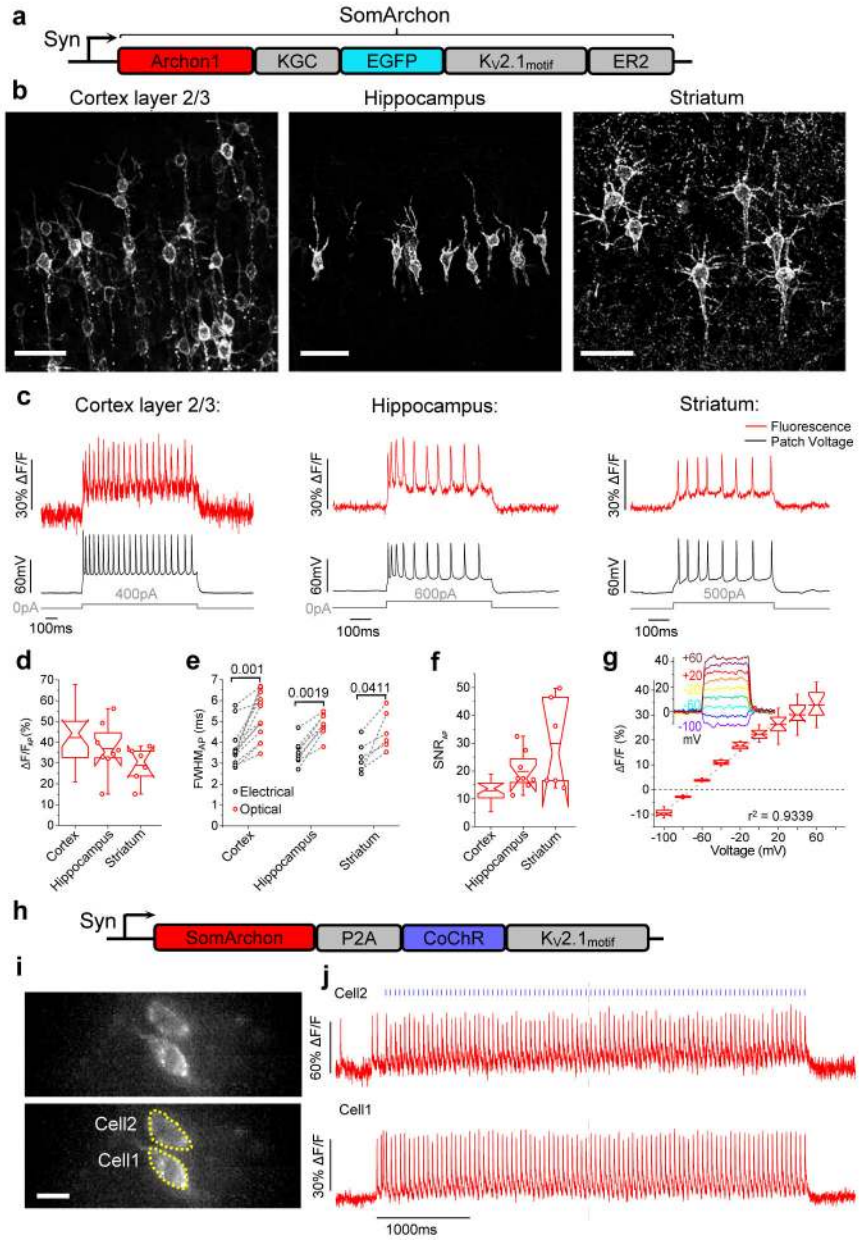

Figure 1. SomArchon enables high fidelity voltage imaging in brain slices.

(**a**) Diagram of the SomArchon construct. (**b**) Confocal images of SomArchon expressing neurons in cortex layer 2/3 (left), hippocampus (middle), and striatum (right). λ_{ex}=488nm laser, λ_{em}=525/50 nm (representative images selected from 8, 10, and 6 slices from 2 mice each, respectively). Scale bars, 50 μm. (**c**) Single-trial SomArchon fluorescence (red), and concurrently recorded membrane voltage via whole-cell patch-clamp (black), during current injection (gray) evoked action potentials (APs); λ_{ex}=637nm laser at 0.8, 1.5, and 1.5 W/mm^2 for cortex, hippocampus, and striatum, respectively. (**d**) ΔF/F per AP across recordings exemplified in **c** (representative traces selected from n = 18, 8, and 6 neurons from 5, 2, and 2 mice, respectively). Box plots (25th and 75th percentiles with notch being the median; whiskers extend 1.5x the interquartile range from the 25th and 75th percentiles;

middle horizontal line, mean; individual data points shown as open circles when n < 9). (**e**) Electrical and optical AP waveform full-width-at-half-maximum (FWHM; dashed lines connect same neurons) across recordings exemplified in **c** (*p*-values are from two-sided Wilcoxon rank sum test, see Supplementary Table 2). (**f**) SNR per AP across recordings exemplified in **c**. (**g**) Population fluorescence of SomArchon in response to voltage steps in voltage-clamp mode, normalized to the fluorescence at −70 mV (optical recordings for a representative neuron shown in inset) recorded in cortex (n=12 neurons from 2 mice). (**h**) Diagram of SomArchon-P2A-CoChR-$K_V2.1_{motif}$. (**i**) Fluorescence image of neurons in hippocampal slice, expressing SomArchon-P2A-CoChR-$K_V2.1_{motif}$ (top) with two cells identified (bottom); λ_{ex}=637 nm, exposure time 1.3 ms (selected from n=3 slices from 2 mice). Scale bar = 25 μm. (**j**) Representative single-trial optical voltage traces from cells shown in **i** with blue light stimulation (2 ms pulse at 20 Hz). Acquisition rate: 777 Hz.

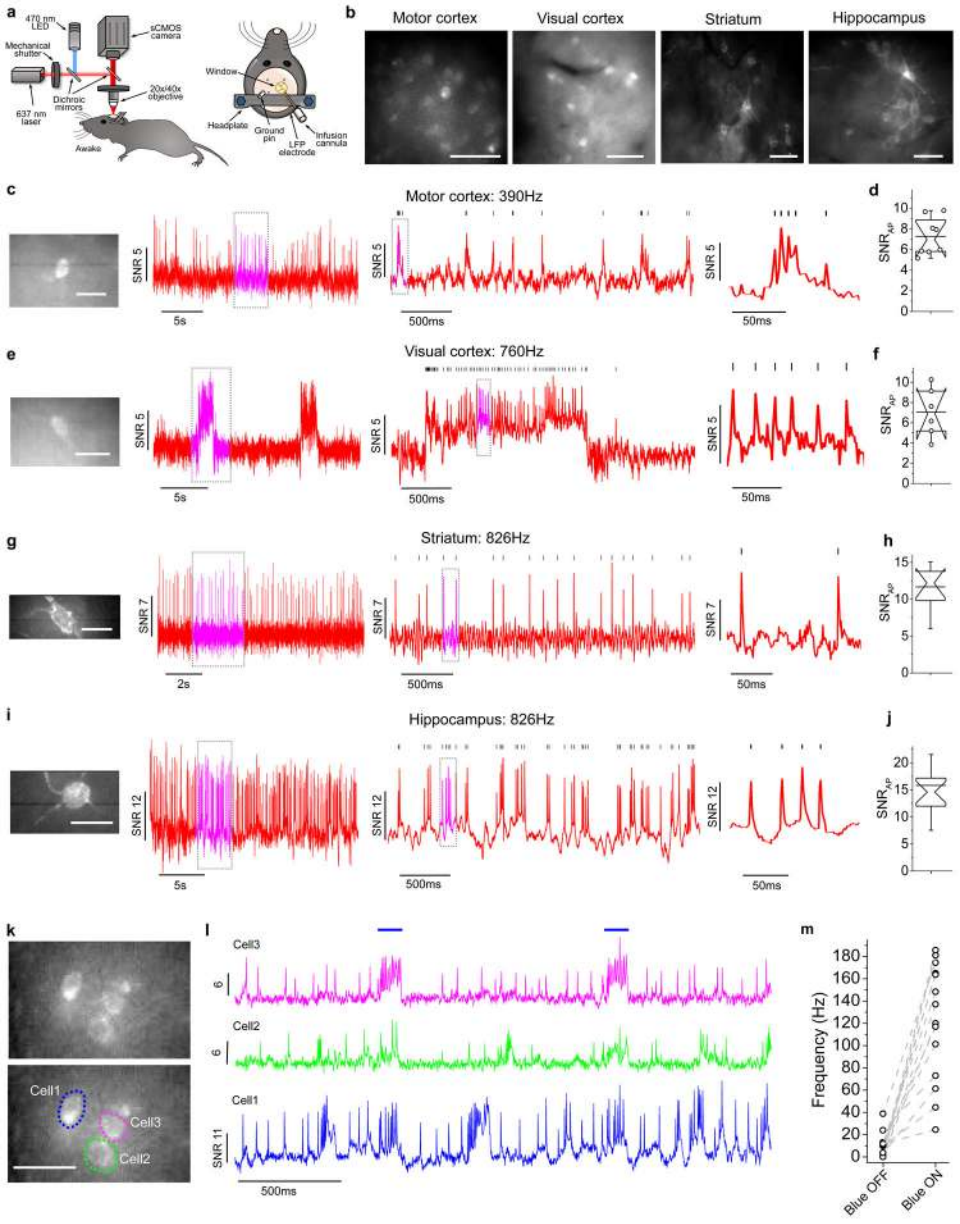

Figure 2. SomArchon enables single cell voltage imaging in multiple brain regions of awake mice, using a simple wide-field imaging setup.

(**a**) Experimental setup: awake mice were head-fixed under a wide-field microscope (left); diagram of surgical window implant coupled with an infusion cannula and an LFP recording electrode (right). (**b**) Representative SomArchon-expressing neurons visualized via EGFP fluorescence in motor cortex, visual cortex, striatum, and hippocampus (λ_{ex}=470/25 nm LED, λ_{em}=525/50 nm;). Scale bars, 50 μm. (**c**, **e**, **g**, **i**) Voltage imaging in (**c**) motor cortex, (**e**) visual cortex, (**g**) striatum, and (**i**) hippocampus. SomArchon fluorescence image of the cell *in vivo* (left) and optical voltage trace acquired from the cell (right; dashed boxes indicate time intervals shown at successively expanded time scales; vertical bars indicate peaks of action potentials identified by a custom spike-sorting algorithm); λ_{ex}=637 nm laser, at 1.6 W/mm^2 for visual cortex and motor cortex, 4 W/mm^2 for striatum and

hippocampus, λ_{em}=664LP). Scale bars, 25 μm. (**d, f, h, j**) Quantification of SNR per action potential for (**d**) motor cortex, (**f**) visual cortex, (**h**) striatum, and (**j**) hippocampus. Box plots are displayed as described in Fig. 1. In **b-j**, representative images and traces were selected from, and statistics performed on, n = 8, 6, 10, and 17 cells from 3, 2, 3, and 4 mice respectively. (**k**) Fluorescence image of selected FOV showing hippocampal neurons expressing SomArchon-P2A-CoChR-$K_V2.1_{motif}$ (top) with neurons identified (bottom); λ_{ex}=637 nm, exposure time 1.2 ms. Scale bar, 20 μm. (**i**) Representative single-trial optical voltage traces from cells shown in **k** with blue light stimulation (100 ms pulse). Image acquisition rate: 826 Hz. (**m**) Firing rate changes during blue light off versus blue light on conditions in individual neurons. In **k-m,** representative image selected from, and statistics performed on, n = 14 cells from 2 mice.

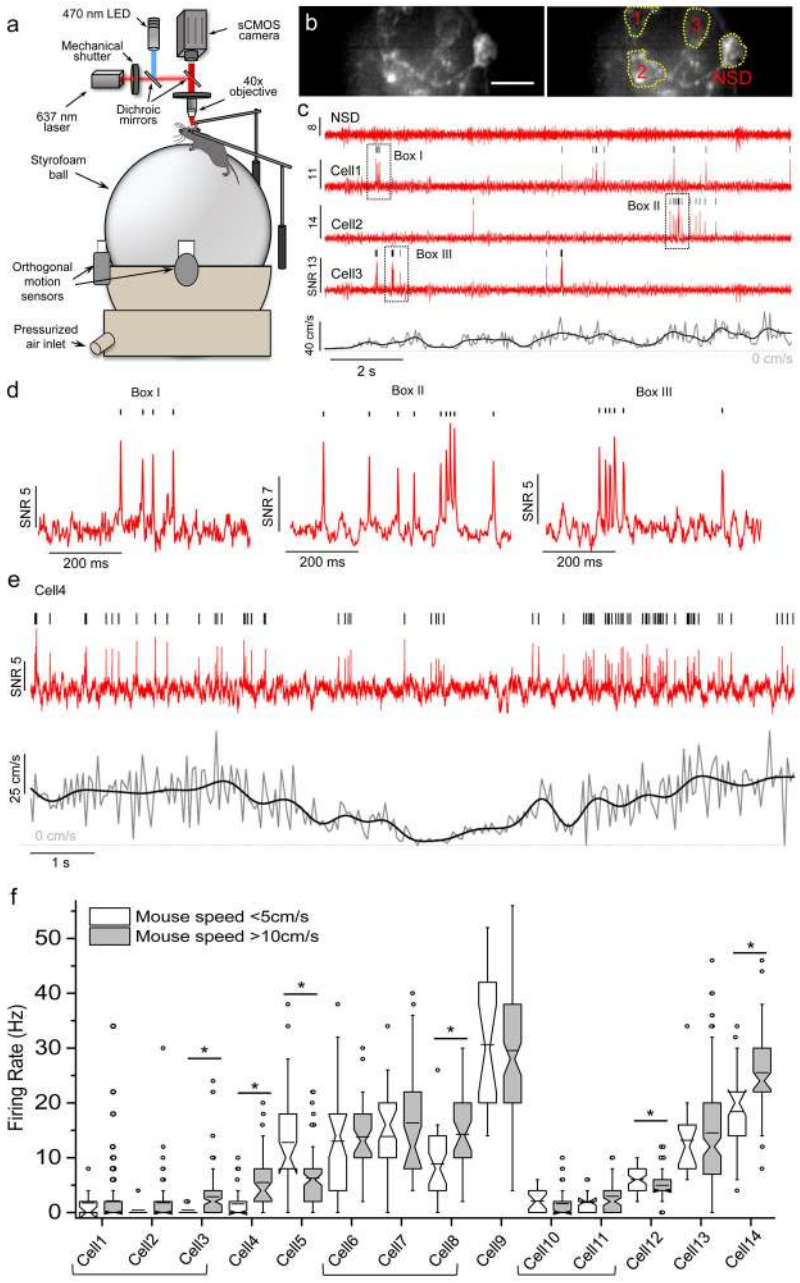

Figure 3. Voltage imaging of striatal neurons during locomotion.

(**a**) Schematic representation of the experimental setup, similar to that in Figure 2a, but with mice positioned on a spherical treadmill. Imaging was performed with a 40x objective lens. (**b**) SomArchon fluorescence image of striatal cells (left), with identified ROIs corresponding to somas (right), λ_{ex}=637 nm, exposure time 1.2 ms (representative image selected from n = 9 FOV from 2 mice). Scale bar, 20 μm. NSD: no spikes detected. (**c**) Optical voltage traces acquired from cells shown in **b**, and corresponding mouse movement speed (black: low pass filtered at 1.5 Hz; gray: raw data; representative traces selected from n = 2 FOV from one mouse). Image acquisition rate, 826 Hz. (**d**) Zoomed-in views of the three periods indicated by black boxes shown in **c**. (**e**) Optical voltage trace (red) for a

neuron modulated by movement speed and corresponding movement speed (black) (representative trace selected from n = 14 neurons from 2 mice). (**f**) Firing rates of individual striatal neurons, during periods with low (open box) versus high (gray) movement speed (n=14 neurons from 2 mice, brackets indicate neurons from the same FOV). *, $p<0.05$, two-sided Wilcoxon rank sum test. Box plots are displayed as described in Fig. 1.

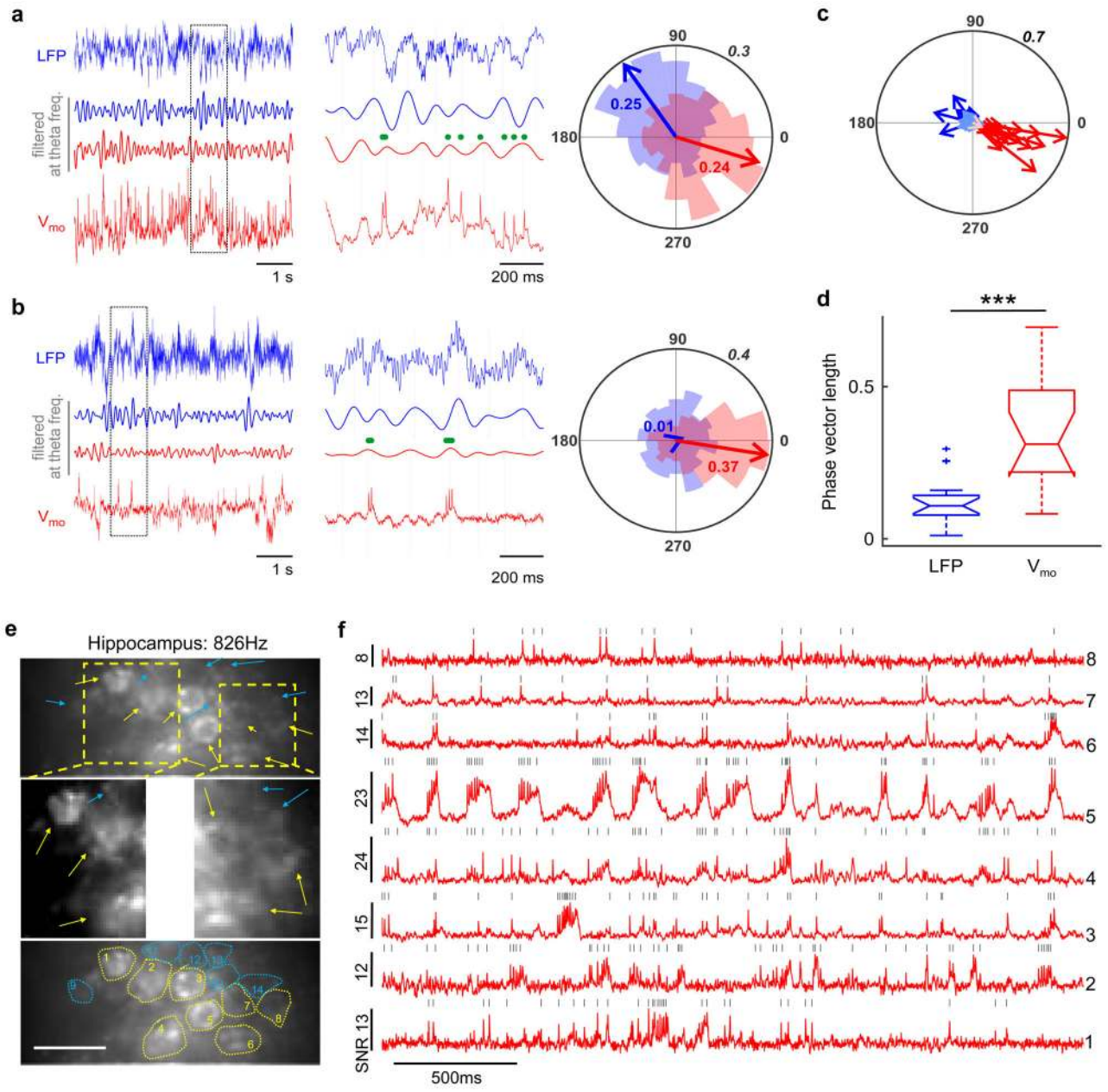

Figure 4. Population voltage imaging of spikes and subthreshold voltage activities in CA1 neurons.

(**a**) A neuron with spikes phase-locked to theta oscillations of local field potentials (LFPs, blue) and optically-recorded membrane voltage (V_{mo}, red). (Left) Raw LFPs (top) and V_{mo} (bottom), and theta frequency filtered traces (middle). (Center) Zoomed-in view of the boxed period on the left. Theta oscillation peaks are indicated by blue and red vertical lines, and spikes by green dots. (Right) Probability distribution of spikes to theta oscillation phases of LFP (blue) and V_{mo} (red). Arrows indicate the average phase vector (with vector length indicated). Outer circle number indicates probability. (Example is selected from n=16 neurons in 7 FOVs from 4 mice) (**b**) As in (**a**), but for an example neuron phase locked to V_{mo} theta oscillations, but not to LFP theta oscillations. (**c**) Population spike-phase vectors

to theta oscillations of LFP (blue and light blue) and V_{mo} (red and pink). Each vector represents the average vector from one neuron (blue and red: $p<0.05$; light blue and pink: not significant; χ^2 test, spike-phase distribution of each neuron against uniform distribution; n = 198–1077 spikes per neuron; 16 neurons in 7 FOVs from 4 mice). (**d**) Population spike-phase relationship. (***, $p = 5.0 \cdot 10^{-5}$, two-tailed paired Student's t-test, n=16 neurons in 7 FOVs from 4 mice). Box plots (25th and 75th percentiles with notch being the median; whiskers extend to all data points not considered outliers; + are outliers. (**e**) SomArchon fluorescence images of CA1 neurons (left), with ROIs overlaid (right) (n = 14 FOV from 3 mice). Example spiking cells are indicated by yellow arrows whose optical voltage traces are shown in (**f**); blue arrows indicate neurons not active during the period shown; λ_{ex}=637 nm laser at 1.5 W/mm^2. Scale bar, 20 μm.